
CMS Physics Analysis Summary

Contact: cms-pag-conveners-higgs@cern.ch

2011/07/23

Search for standard model Higgs boson in pp collisions at $\sqrt{s} = 7$ TeV

The CMS Collaboration

Abstract

The overall combination is presented of six standard model (SM) Higgs boson searches performed by the CMS Collaboration using the following Higgs boson decay signatures: $H \rightarrow \gamma\gamma$, $H \rightarrow \tau\tau$, $H \rightarrow WW \rightarrow 2\ell 2\nu$, $H \rightarrow ZZ \rightarrow 4\ell$, $H \rightarrow ZZ \rightarrow 2\ell 2\nu$, and $H \rightarrow ZZ \rightarrow 2\ell 2q$. Depending on the analysis, the amount of data used corresponds to 1.0-1.1 fb⁻¹ of integrated luminosity. The conclusion of this combination is that the SM Higgs boson is excluded at 95% C.L. in two mass ranges 149-206 and 300-440 GeV/ c^2 , as well as several narrower intervals in between. The expected exclusion in the absence of a signal is 127-420 GeV/ c^2 . At 90% C.L., we exclude the SM Higgs boson in the mass range from 145-480 GeV/ c^2 . The same experimental search results, reinterpreted in the context of the standard model with 4 fermion generations (SM4), allow us to exclude the SM4 Higgs boson with a mass in the range 120-600 GeV/ c^2 at 95% C.L.

1 Introduction

The discovery of the mechanism for electroweak symmetry breaking is one of the key parts of the Large Hadron Collider (LHC) physics program. In the standard model (SM), this can be achieved by invoking what has become known as the Higgs mechanism, leading to the prediction of the Higgs boson. The Higgs boson mass is essentially the only unknown in the model, all other parameters being reasonably well constrained by existing measurements. To date, the experimental searches for this elusive particle have yielded negative results and limits on its mass have been placed by experiments at LEP, $m_H > 114.4 \text{ GeV}/c^2$ [1], and the Tevatron, $m_H < 158$ or $m_H > 173 \text{ GeV}/c^2$ [2]. Fits of the electroweak precision measurements, not taking into account the direct search results, constrain indirectly the SM Higgs boson mass to be relatively light, $m_H < 158 \text{ GeV}/c^2$ [3]. All limits quoted in this note are at 95% C.L. unless explicitly stated otherwise.

The CMS Experiment [4] was designed to be able to detect a Higgs boson with a mass ranging from the LEP lower mass bound up to roughly $1 \text{ TeV}/c^2$. Depending on the Higgs boson mass various production mechanisms and decay channels are possible and are actively being pursued. In this note, we report the overall combination of the search results obtained in the following six analyses, grouped by the Higgs decay modes: $H \rightarrow \gamma\gamma$ [5], $H \rightarrow \tau\tau$ [6], $H \rightarrow WW \rightarrow 2\ell 2\nu$ [7], $H \rightarrow ZZ \rightarrow 4\ell$ [8], $H \rightarrow ZZ \rightarrow 2\ell 2\nu$ [9], and $H \rightarrow ZZ \rightarrow 2\ell 2q$ [10]. Each of these analyses has a number of sub-channels that add up to a total of 30 independent signatures entering the overall combination. The choice of the Higgs boson mass points used in the analyses and the overall combination is driven by either instrumental $\gamma\gamma/4\ell$ mass resolutions (for $m_H < 250 \text{ GeV}/c^2$) or by the expected standard model Higgs boson width at higher masses.

The cross sections, together with their uncertainties, for each Higgs boson production mechanism and decay branching ratios are taken from the CERN Yellow Report prepared by the LHC Higgs Cross Section Group [11]. The gg -fusion cross section is calculated at NNLO_{QCD} + NNLL_{QCD} + NLO_{EWK} precision, the vector boson fusion (VBF) and the associated WH and ZH cross sections—at NNLO_{QCD} + NLO_{EWK} precision, while $t\bar{t}H$ —at NLO_{QCD} precision. The errors on the branching ratios are generally very small and have been neglected in most of the analyses presented in this note. Uncertainties on the Higgs boson mass lineshape and its impact on the cross section for a Higgs boson with very large mass ($m_H > 400 \text{ GeV}/c^2$) are not yet included.

In Section 2, we briefly outline the overall statistical model used in this work. In Section 3, we give a brief overview of each analysis entering the overall combination. And finally, in Section 4, we present our main results.

2 Statistical Analysis

A statistical combination of results of multiple searches furthers the overall experimental sensitivity to the presence or absence of new physics in comparison to what otherwise could be inferred from each analysis on its own. The challenge of such an undertaking is to put all analyses in the same framework and understand the role of different systematic errors, including their inter-channel correlations. In this section, we describe our choices for modeling systematic errors in general and which ones we would treat as correlated, in particular. We also give a brief summary of the statistical methods and software tools we use for quantifying the search results presented in this note.

Notations

In the following, the expected SM Higgs event yields are generically denoted as s , and backgrounds as b . These stand for event counts in one or multiple bins or for probability density functions, whichever is used in an analysis. Predictions for both signal and background yields, prior to the scrutiny of the data entering the statistical analysis, are subject to multiple uncertainties that are handled by introducing nuisance parameters θ , so that signal and background expectations become functions of the nuisance parameters: $s(\theta)$ and $b(\theta)$. The events actually observed are denoted as an *observation*. It has become customary to represent the negative SM Higgs search results as limits on a common *signal strength modifier* μ that is taken to change the cross sections of all production mechanisms by exactly the same scale.

Modeling of systematic errors

We follow the procedure detailed in Ref. [12]. All systematic errors are treated as either 100% correlated (positively or negatively) or independent. Partially correlated errors are broken further down to independent sources or declared to be correlated/uncorrelated, whichever is judged to be a better approximation or more conservative. Each independent source of uncertainties is associated to a nuisance parameter θ . Correlated errors driven by the same nuisance parameter need not have the same scale.

For the calculations described below, we need to model the sources of uncertainty. This is done with the help of priors in Bayesian calculations, and measurement *pdfs* in frequentist ones. Below are the types of priors $\rho(\theta | \tilde{\theta})$ used in combination presented in this note. Their frequentist counterpart *pdfs* are introduced in the next sub-section.

- Nuisance parameters, unconstrained by any a priori considerations and/or measurements, are assigned *flat priors*.
- Nuisance parameters that can take both positive and negative values are generally described by *Gaussian distributions* with some mean value $\tilde{\theta}$ and width parameter σ .
- Systematic errors on observables that can take only positive values (cross sections, luminosity, selection efficiencies, etc.) are generally described by *log-normal distributions*. They are characterized by the parameter κ , a factor by which the true value of an observable can be larger or smaller than its default. Technically, log-normal errors are modeled by writing an observable A in the following form $A = A_0 \cdot \kappa^\theta$, where θ is a nuisance with the normal *pdf*. In other words, log-normal errors can be and are handled via normal *pdf* constraints.
- Uncertainties of statistical nature (e.g., statistical error associated with a number of events simulated in MC or a number of observed events in a control region) are described with *gamma distributions*. The width of the gamma distribution is determined by the number of simulated or observed events.

Modified frequentist limits (CL_s)

As the prime method for reporting limits in this note, we use the modified frequentist construction (often referred to as CL_s) [13, 14]. To fully define the method, one needs to make a choice of the test statistic and how one would treat nuisance parameters in the construction of the test statistic and in generating pseudo-data. In this note, we follow the prescription prepared by the LHC Higgs Combination Group [12]. Below is a brief outline of the procedure.

The first step is to re-interpret systematic error *pdfs* $\rho(\theta | \tilde{\theta})$ as posteriors arising from some

“real” or “imaginary” measurements $\tilde{\theta}$, as given by the Bayes’ theorem:

$$\rho(\theta|\tilde{\theta}) \sim p(\tilde{\theta}|\theta) \cdot \pi_{\theta}(\theta), \quad (1)$$

where $\pi_{\theta}(\theta)$ functions are hyper-priors for those “measurements”. These hyper-priors are chosen to be uniform (flat) distributions. With this choice, $\rho(\theta|\tilde{\theta})$ will be a gamma distribution, if $p(\tilde{\theta}|\theta)$ is Poisson, and normal or log-normal if $p(\tilde{\theta}|\theta)$ is normal. This approach allows sampling distributions for the test statistic to be constructed in a purely frequentist manner.

The likelihood $\mathcal{L}(\text{data}|\mu, \theta)$ to be used in constructing the test statistic is defined as follows:

$$\mathcal{L}(\text{data}|\mu, \theta) = \text{Poisson}(\text{data}|\mu \cdot s(\theta) + b(\theta)) \cdot p(\tilde{\theta}|\theta), \quad (2)$$

where $\text{Poisson}(\text{data}|\mu s(\theta) + b(\theta))$ is the Poisson probability to observe *data*, assuming signal and background models, $s(\theta)$ and $b(\theta)$, that depend on some nuisance parameters θ .

The test statistic is then defined as the profile likelihood ratio:

$$q_{\mu} = -2 \ln \frac{\mathcal{L}(\text{data}|\mu, \hat{\theta}_{\mu})}{\mathcal{L}(\text{data}|\hat{\mu}, \hat{\theta})}, \quad \text{with a constraint } 0 \leq \hat{\mu} \leq \mu \quad (3)$$

where “data” can be the actual *observation* or pseudo-data. Both the denominator and numerator are maximized. In the numerator, μ remains fixed and only the nuisance parameters θ are allowed to float. Their values at which \mathcal{L} reaches the maximum are denoted as $\hat{\theta}_{\mu}$. In the denominator, both μ and θ are allowed to float in the fit, and $\hat{\mu}$ and $\hat{\theta}$ are parameters at which \mathcal{L} reaches its global maximum. The lower constraint on $\hat{\mu}$ ($0 \leq \hat{\mu}$) is imposed by hand as the signal rate cannot be negative. The upper constraint ($\hat{\mu} \leq \mu$) forces the limit to be one-sided. For observations preferring the best-fit values of $\hat{\mu} > \mu$, the test statistic collapses to zero. The value of the test statistic for the actual observation will be denoted as q_{μ}^{obs} .

Next, we find the values of nuisance parameters $\hat{\theta}_0^{\text{obs}}$ and $\hat{\theta}_{\mu}^{\text{obs}}$ best describing the experimentally *observed* data (i.e. maximizing \mathcal{L}), for the *background-only* and *signal+background* hypotheses, respectively. Using these best-fit values of nuisance parameters, we generate toy Monte Carlo pseudo-data to construct the test statistic *pdfs* assuming a signal with strength μ and for the *background-only* hypothesis ($\mu = 0$). The “measurements” $\tilde{\theta}$ are also randomized in each pseudo-data, using the *pdfs* $p(\tilde{\theta}|\theta)$ from Eq. (1). Note, that for the purposes of *pseudo-data generation*, the nuisance parameters are fixed to their data-driven best-fit values $\hat{\theta}_{\mu}^{\text{obs}}$ or $\hat{\theta}_0^{\text{obs}}$, but are allowed to float in fits needed to evaluate the test statistic. An example of two such sampling *pdfs* is given in Fig. 1 (left). These sampling distributions are obtained for the actual combination for a Higgs boson mass $m_H = 250 \text{ GeV}/c^2$.

Having constructed two such *pdfs*, we find two *p*-values to be associated with the actual observation for the *signal+background* and *background-only* hypotheses, p_{μ} and p_0 :

$$p_{\mu} = P\left(q_{\mu} \geq q_{\mu}^{\text{obs}} \mid \mu s(\hat{\theta}_{\mu}^{\text{obs}}) + b(\hat{\theta}_{\mu}^{\text{obs}})\right), \quad (4)$$

$$p_0 = P\left(q_{\mu} \geq q_{\mu}^{\text{obs}} \mid b(\hat{\theta}_0^{\text{obs}})\right), \quad (5)$$

and calculate $\text{CL}_s(\mu)$ as a ratio of these two *p*-values,

$$\text{CL}_s(\mu) = \frac{p_{\mu}}{p_0}. \quad (6)$$

If for $\mu = 1$ $CL_s = \alpha$, we say that the SM Higgs boson is excluded at the $(1 - \alpha)$ Confidence Level (C.L.). It is known that the CL_s method gives conservative limits, i.e. the actual confidence level is higher than $(1 - \alpha)$.

To quote the 95% Confidence Level upper limit on μ , to be further denoted as $\mu^{95\%CL}$, we adjust μ until we reach $CL_s = 0.05$.

The detailed discussion of differences between the three flavors of CL_s , LEP-type [15], Tevatron-type [16–18], and the one defined by the LHC Higgs Combination group (and briefly outlined above), can be found elsewhere [12]. In brief, the main differences are:

- Both LEP and Tevatron used the test statistic with fixed $\mu = 0$ in the denominator (cf. Eq. 3), which does not guarantee the desired asymptotic behavior allowing to approximately evaluate p -values from the value of the observed test statistic itself, without having to generate large amounts of pseudo-data.
- LEP did not profile systematic errors in the test statistic, which does not allow one to take advantage of the constraints arising from the data used in the statistical analysis. Tevatron does profile systematic errors as we do.
- Both LEP and Tevatron used a Bayesian-frequentist approach to handling systematic errors in generating sampling distributions, while we use a pure frequentist approach.

Numerically, results derived from the Tevatron-type and LHC-type CL_s definitions are found to be very similar.

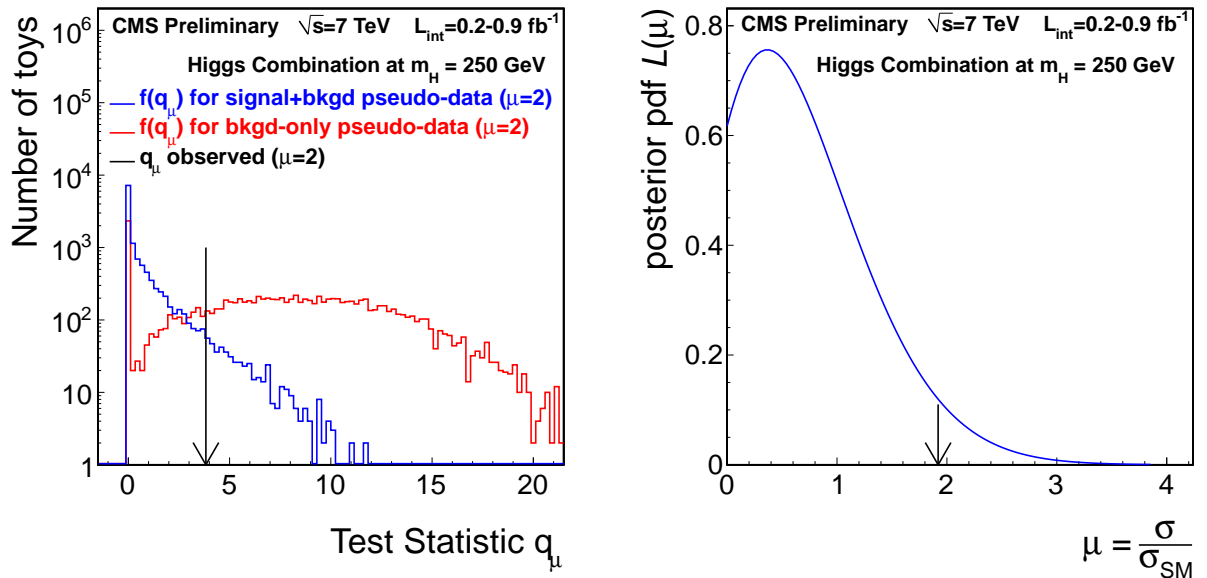


Figure 1: (Left) Frequentist tests statistic q_μ for distributions for ensembles of pseudo-data generated for *background-only* and *signal+background* hypotheses. The signal strength assumed in this example is $\mu = 2$. The observed value of the test statistic q_μ^{obs} is indicated by the arrow. Probabilities to find an observation above this value for the *background-only* and *signal+background* hypotheses are $p_0 = 0.868 \pm 0.005$ and $p_\mu = 0.040 \pm 0.002$, respectively, resulting in $CL_s = p_\mu / p_0 = 0.046 \pm 0.002$. (Right) Bayesian posterior $L(\mu | data)$. The value of $\mu^{95\%CL}$ is indicated by the arrow.

Bayesian limits

As an alternative to the CL_s method, we also use the Bayesian approach. In this method, Bayes' theorem [19] is invoked to assign a degree of belief to the Higgs hypothesis by calculating the posterior "probability density function" $p(\mu | \text{data})$ on the signal strength μ :

$$p(\mu | \text{data}) = \frac{1}{C} \int_{\theta} p(\text{data} | \mu s(\theta) + b(\theta)) \rho_{\theta}(\theta) \pi_{\mu}(\mu) d\theta. \quad (7)$$

Functions $\rho_{\theta}(\theta)$ are *pdfs* describing our prior belief on the scale and description of uncertainties, or systematic errors. The function $\pi_{\mu}(\mu)$ is the prior on the signal strength, which we take to be flat for $\mu \geq 0$ and zero otherwise. The constant C is set to normalize the overall posterior function $p(\mu | \text{data})$ to unity. An example of the posterior $p(\mu | \text{data})$ for the actual combination at the mass point $m_H = 250 \text{ GeV}/c^2$ is shown in Fig. 1 (right). Integration over nuisance parameters in the above equation is called marginalization. The Bayesian one-sided 95% C.L. limits on μ are extracted from the following equation:

$$\int_0^{\mu_{95\%CL}} p(\mu | \text{data}) d\mu = 0.95 \quad (8)$$

Quantifying significance of an excess of events

In anticipation of the eventual Higgs boson discovery, we produce a scan of an approximate local \tilde{p} -value characterizing a scale of all observed excesses vs hypothesized Higgs boson mass m_H . The approximate \tilde{p} -value is derived from the asymptotic properties of the test statistic based on the profile likelihood ratio [20]:

$$\tilde{p} = \frac{1}{2} \left[1 - \text{erf} \left(\sqrt{q_0^{\text{obs}}/2} \right) \right] \quad (9)$$

where q_0^{obs} is the observed test statistic calculated for $\mu = 0$ and with only one constraint $0 \leq \hat{\mu}$, which ensures that data deficits are not counted on an equal footing with data excesses. The approximation has been tested and works well for the range of expected background and signal yields expected. Figure 2 gives an example of the distribution of the test statistic q_0 . One can see that the test statistic sampling distribution agrees well with the approximation shown as a curve. This sampling distribution is obtained for the actual combination for a Higgs boson mass $m_H = 250 \text{ GeV}/c^2$.

To quote significance, we choose a "one-sided Gaussian" convention for associating p -value and significance Z as follows:

$$p = \int_Z^{\infty} \frac{1}{\sqrt{2\pi}} \exp(-x^2/2) dx. \quad (10)$$

Should we start seeing the build-up of a significant excess of events at any particular Higgs boson mass, procedures exist for more accurate characterization of local p -values and assessing the look-elsewhere effect. They are defined in the LHC Higgs Combination Group Report [12]

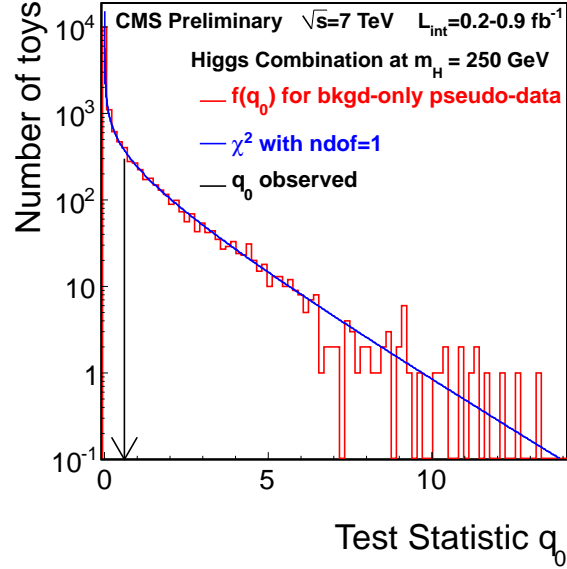


Figure 2: Frequentist tests statistic q_0 for distributions for ensemble of pseudo-data generated for *background-only* hypotheses. The curve is the asymptotic χ^2 distribution for one degree of freedom. The observed value of the test statistic q_0^{obs} is indicated by the arrow. The true p -value of such an observation, i.e. probability $P(q_0 \geq q_0^{obs})$, as obtained from the sampling distribution is 0.180 ± 0.004 , while the approximate \tilde{p} -value, as given by Eq. (9), is 0.218.

Statistical analysis tools

All results quoted in this paper are validated by using two independent sets of software tools, RooStats [21] and L&S [22]. Both have been made to run off the same input information provided by the individual analyses for each channel. The agreement of numbers obtained with two very different software implementations is indicative of their computational robustness. In addition, many cross checks were done between the independent combination tools of CMS and ATLAS in terms of reproducibility for a large set of test scenarios [12]. The computational precision on all results reported in this note is at the level of $O(1\%)$ of the quoted numbers, unless stated otherwise.

3 Search channels used in the combination

The combination presented in this note is based on six major channels classified by the final Higgs decay chain signature as shown in Table 1. The mass search regions are specific to each analysis. The analyzed integrated luminosity varies somewhat from channel to channel and is typically about 1.1 fb^{-1} .

From Table 1, one can also see that different analysis strategies are employed in different searches. They include three basic types: cut-and-count analyses, analyses of binned distributions, and unbinned analyses tracking individual events and using parametric models of signal and background shapes.

The last column in Table 1 shows the number of nuisance parameters (systematic errors) in each analysis. The total number of independent nuisance parameters in the current combination is 142. All systematic errors can be classified in two main groups: those expected to be correlated between different searches (24) and remaining ones specific to individual analyses (118)¹. Table 2 shows the full list of correlated errors that appear in the current combination. The top block in the table is a subset of the list prepared by the LHC Higgs Combination Group [12]. The bottom block are correlated errors that are correlated within CMS only. Quantities affected by the uncertainties listed in Table 2 are all positively defined and, hence, modeled as log-normals.

In the following subsections, we give a brief description of search strategies for the six channels used in this combination. Detailed information can be found in references provided within each sub-section.

Table 1: Summary information on the analyses included in the combination. The first number in the last column gives the number of nuisance parameters correlated across two or more analyses. The second number refers to the number of nuisance parameters specific to one analysis only.

channel	mass range (GeV/ c^2)	luminosity (fb^{-1})	number of sub-channels	type of analysis	number of nuisances
$H \rightarrow \gamma\gamma$	110-140	1.1	8	mass shape (unbinned)	3+40=43
$H \rightarrow \tau\tau$	110-140	1.1	6	mass shape (binned)	10+21=31
$H \rightarrow WW \rightarrow 2\ell 2\nu$	110-600	1.1	5	MVA (binned); cut&count	16+36=52
$H \rightarrow ZZ \rightarrow 4\ell$	110-600	1.1	3	mass shape (unbinned)	12+7=19
$H \rightarrow ZZ \rightarrow 2\ell 2\nu$	250-600	1.1	2	cut&count	14+4=18
$H \rightarrow ZZ \rightarrow 2\ell 2q$	226-600	1.0	6	mass shape (unbinned)	13+10=23
TOTAL (6)	110-600	1.0-1.1	30		24+118=142

¹The majority of them are actually also correlated between different sub-channels within an analysis.

Table 2: Correlated systematic errors in the analyses contributing to the combination. Uncertainties associated with the photon reconstruction are not in the table as they appear only in one analysis.

group	nuisance	comments
cross section (pdf)	gg qqbar	$gg \rightarrow H, t\bar{t}H, VQQ, t\bar{t}, tW, tb$ (s-channel), $gg \rightarrow VV$ VBF $H, VH, V, VV, \gamma\gamma$
cross section (QCD scales)	ggH ggH1in ggH2in qqH VH ttH VV ggVV	total inclusive $gg \rightarrow H$ inclusive $gg/qg \rightarrow H + \geq 1$ jets inclusive $gg/qg \rightarrow H + \geq 2$ jets VBF H associate VH $t\bar{t}H$ WW, WZ, and ZZ up to NLO $gg \rightarrow WW$ and $gg \rightarrow ZZ$
phenomenology	UE & PS	modeling of underlying event (UE) and parton showering (PS)
luminosity	lumi	uncertainties in luminosity
efficiencies	muon electron tau b-tag	prompt muon efficiency (includes reconstruction, isolation) prompt electron efficiency (includes reconstruction, isolation) reconstruction efficiency of prompt hadronically decaying tau b-tag efficiency for b-jets (anti-correlated with b-jet veto)
p_T scales	muon electron tau jets	prompt muon p_T -scale error prompt electron p_T -scale error p_T scale error for prompt hadronically decaying tau jet energy scale error
p_T resolutions	electron	prompt electron p_T -resolution error
fake rates	lepton	systematic errors associated with determination of fake lepton rates in data
trigger efficiencies	muon electron	prompt muon efficiency (includes trigger, reconstruction, isolation) prompt electron efficiency (includes trigger, reconstruction, isolation)

3.1 $H \rightarrow \gamma\gamma$ channel [5]

In this channel, the signal of a standard model Higgs boson is a narrow peak in the diphoton invariant mass distribution ($m_{\gamma\gamma}$), dominated by experimental resolutions, on a large falling background spectrum.

Events are first selected by requiring a diphoton trigger to have fired. Photon candidates, isolated in the tracking detectors and calorimeters, are required to pass a set of tight identification and quality cuts, reducing the background contributions from events with fake photons. Photon candidates must have a pseudorapidity, within the acceptance of the detector: $|\eta| < 2.5$ and outside the transition region between the barrel and endcap detectors: $1.4442 < |\eta| < 1.566$. The two photon candidates with the highest transverse momenta, E_T are selected to form the Higgs candidate and are required to satisfy, $E_T^{\text{lead}} > 40$ GeV and $E_T^{\text{sub-lead}} > 30$ GeV for the leading and sub-leading candidate respectively.

For the data set under consideration, about six interactions per beam crossing, on average, are expected. The choice of reconstructed primary vertex has an impact on the mass resolution and hence on the sensitivity of the analysis. The reconstructed primary vertices are ranked according to the kinematic properties of the relevant charged tracks and the diphoton Higgs candidate. Where there is evidence for a photon having undergone pair production, the associated charged tracks are used to further refine the vertex choice.

The data are split into eight categories based on the eight permutations of whether or not:

- the transverse momentum of the diphoton system $p_T^{\text{Higgs}} > 40$ GeV/ c ;
- both photon candidates are in the barrel detector;
- both photons pass a cut on a discriminant loosely describing the shower shape that will reject photons likely to have undergone a conversion.

Simulated signal events are produced using the next-to-leading-order (NLO) matrix-element generator POWHEG [23] interfaced to PYTHIA [24] for parton showering. Reweighting of the Higgs p_T spectrum is carried out using the NLO+NNLL distribution computed by the HqT program [25]. Smearing of the photon energies is applied to account for differences between data and simulation. These are derived from detailed studies of $Z \rightarrow e^+e^-$ events. The best category di-photons give a peak with $\text{FWHM}/m_H = 2.4\%$ (full width at half maximum), the worst category— $\text{FWHM}/m_H = 6.5\%$. The signal is modelled in the statistical analysis based on a parameterized fit to the smeared and reweighted simulated events, consisting of a sum of two or three Gaussian distributions.

The dominant source of background comes from events containing two real prompt photons or one prompt and a fake from a jet. The contribution from double-fakes is estimated to be small. The background is modelled parametrically directly from unbinned fits to the data using a second order Bernstein [26] polynomials constrained to be positive definite. There is no Monte Carlo input to these fits. Figures 3 and 4 show the binned data, the result of the unbinned fit for the background model (under the null background-only hypothesis), and the parameterized signal distribution (at $5 \times \text{SM}$) for a hypothesized Higgs mass $m_H = 120$ GeV/ c^2 .

Systematic uncertainties on the signal model affecting both the yield and the shape are considered. The largest sources of uncertainty on the event yield arise from the uncertainty on the luminosity (6%).

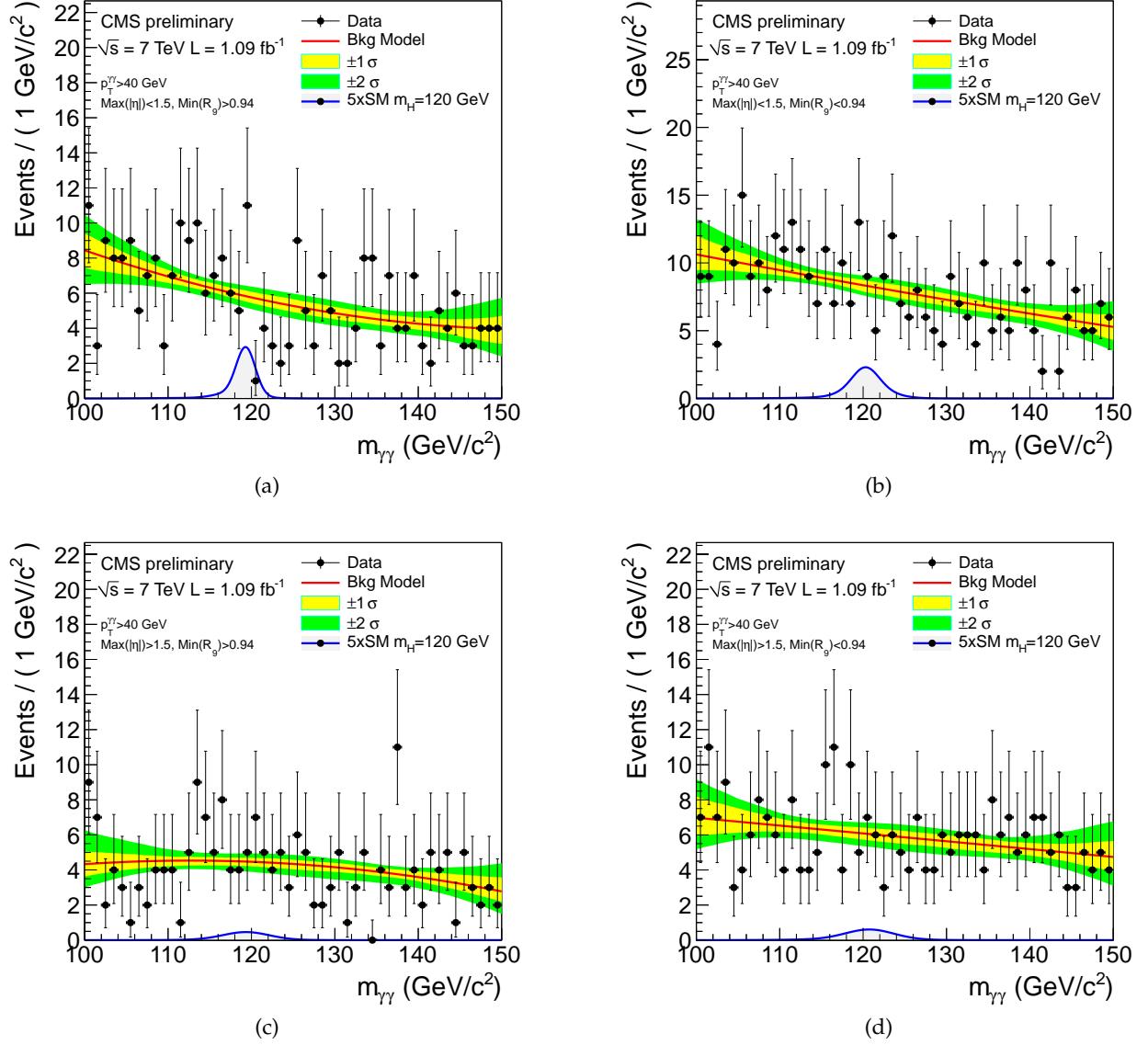


Figure 3: Binned $m_{\gamma\gamma}$ distributions for four event categories for di-photons with $p_T(\gamma\gamma) > 40 \text{ GeV}/c$: (a) Both photons likely unconverted and in the barrel, (b) At least one photon likely to have undergone pair production, both are in the barrel, (c) Both photons likely unconverted and at least one photon in in the endcap, (d) At least one photon likely to have undergone pair production and at least one photon in the endcap. The Monte-Carlo prediction and parameterized signal model for a Higgs boson mass $m_H = 120 \text{ GeV}/c^2$ ($5 \times \text{SM}$) are also shown together with the result of the unbinned fit to the background model. The yellow/green bands indicate $\pm 1\sigma$ and $\pm 2\sigma$ errors on the background fit.

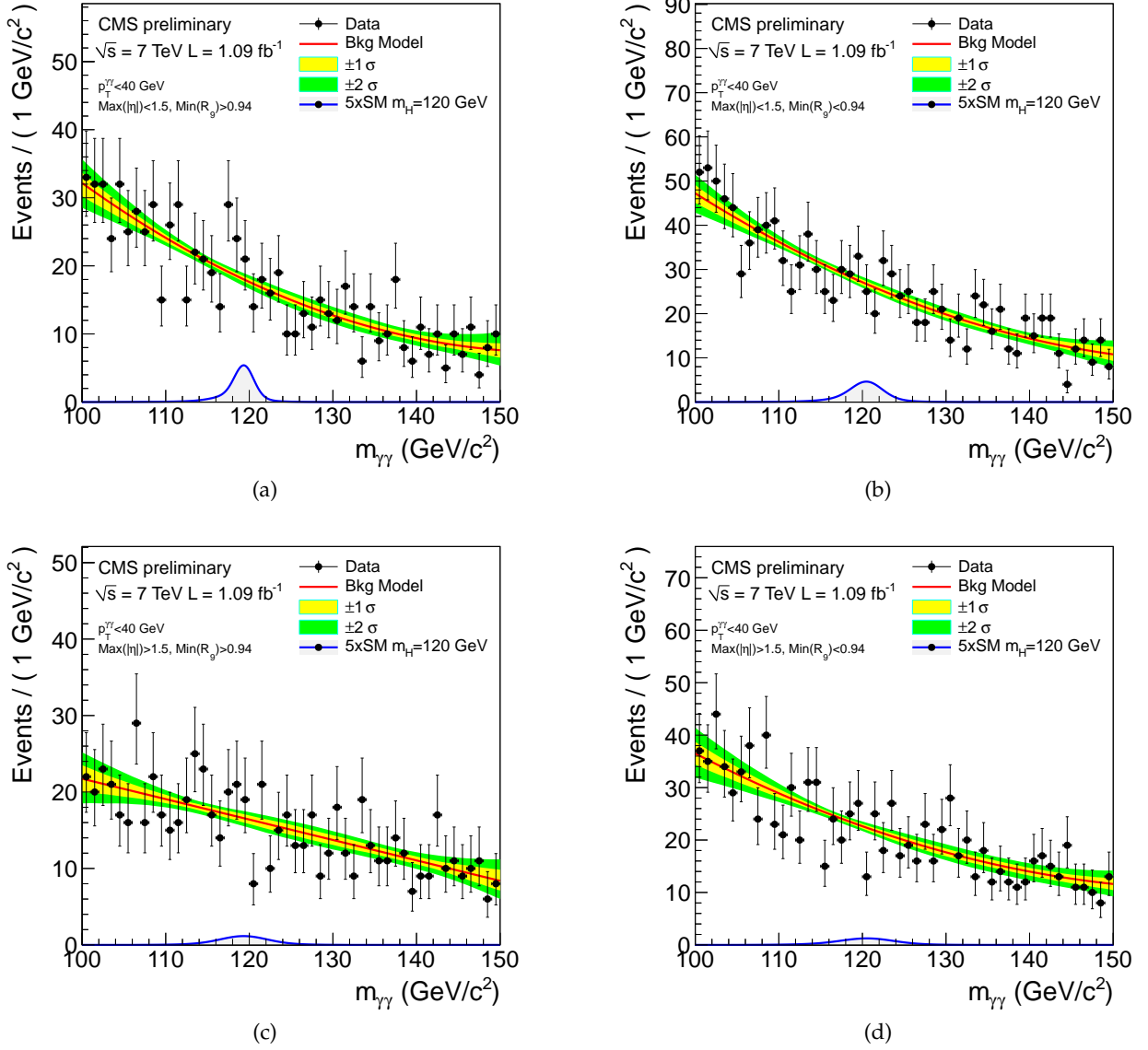


Figure 4: Binned $m_{\gamma\gamma}$ distributions for four event categories for di-photons with $p_T(\gamma\gamma) < 40 \text{ GeV}/c$: (a) Both photons likely unconverted and in the barrel, (b) At least one photon likely to have undergone pair production, both are in the barrel, (c) Both photons likely unconverted and at least one photon in the endcap, (d) At least one photon likely to have undergone pair production and at least one photon in the endcap. The Monte-Carlo prediction and parameterized signal model for a Higgs boson mass $m_H = 120 \text{ GeV}/c^2$ ($5 \times \text{SM}$) are also shown together with the result of the unbinned fit for the background model. The yellow/green bands indicate $\pm 1\sigma$ and $\pm 2\sigma$ errors on the background fit.

3.2 $H \rightarrow \tau\tau$ channel [6]

In this analysis, we search for an excess of events in the visible mass m_{vis} distributions of $e + \tau_{had}$, $\mu + \tau_{had}$ and $e + \mu$ final states², each of which further subdivided in two: with two VBF-like jets or not. Therefore, the search has in total 6 sub-channels. The visible mass is built from measured momenta of electrons, muons, and taus and does not attempt to recover the momentum carried away by neutrinos. The six mass distributions are binned and the entire shape is used in the statistical analysis.

Triggers requiring the presence of both a lepton and an isolated jet consistent with a τ decaying hadronically were adopted for the $e + \tau_{had}$, $\mu + \tau_{had}$ channels. The $e\mu$ events were collected using the di-lepton $e\mu$ trigger. For $e + \tau_{had}$, $\mu + \tau_{had}$ final states, we select events with an isolated electron with $p_T > 20$ GeV/ c or isolated muon with $p_T > 15$ GeV/ c and $|\eta| < 2.1$, and an oppositely charged τ_{had} with $p_T > 20$ GeV/ c and $|\eta| < 2.3$. For the $e\mu$ final state, we select events with an isolated electron with $|\eta| < 2.5$ and an oppositely charged isolated muon with $|\eta| < 2.1$, both with $p_T > 15$ GeV/ c . We reject events with more than one e or μ . A topological cut based on the p_T vectors of the two leptons and the missing transverse energy E_T^{mis} is applied to exploit the fact that visible τ -decay products and neutrinos tend to be colinear.

Motivated by the prominent vector boson fusion component in the Higgs boson production, we split the sample of selected events into two sub-categories as follows:

- VBF: exactly 2 jets with $p_T > 30$ GeV/ c , $m_{jj} > 350$ GeV/ c^2 , $|\Delta\eta_{jj}| > 3.5$, $\eta_1 \cdot \eta_2 < 0$.
- Non-VBF: ≤ 1 jet with $p_T > 30$ GeV/ c , or exactly 2 jets that fail VBF requirements.

The final distribution to discriminate signal from background in each of the six sub-channels is the visible mass m_{vis} . The visible mass distributions for the VBF and non-VBF categories for the $e + \tau_{had}$, $\mu + \tau_{had}$ and $e + \mu$, after all the selection cuts, are shown in Figure 5. The visible mass resolution is about 20%.

The dominant irreducible background in this analysis is $Z \rightarrow \tau\tau$ production. The other three main backgrounds are Electroweak ($W(\ell\nu)$ +jets, $Z(\ell\ell)$ +jets), $t\bar{t}$, and QCD, in which one or both leptons are fakes.

The $Z \rightarrow \tau\tau$ shape is taken from Monte Carlo, while its normalization (total event yield) is constrained by $Z \rightarrow \ell\ell$ measurements and by the fit of the m_{vis} mass shape distribution. The $W(\ell\nu)$ +jets and QCD backgrounds are dealt with by using two control samples: one with the topological cut inverted and another with same-sign di-lepton events. The normalizations for $Z(\ell\ell)$ +jets (important for $e\tau$ -channel), $t\bar{t}$, and di-bosons are taken from corresponding control samples without τ -leptons and scaling them by probabilities for electrons, muons, and jets to fake τ -leptons as measured directly from data.

The largest uncertainties on the signal yield include cross section (12% for ggH and 4% for VBF), luminosity (6%), τ -identification (6%), and jet energy scale (5%). Other errors are O(1%). The largest background uncertainties for VBF categories come from statistical uncertainties for the number of events observed in control samples (up to 40%). For non-VBF selection, the largest background uncertainties are due to extrapolation factors from measurements done in control regions into the signal region: fake rates for electrons (8%) and jets (12%) for $Z(\ell\ell)$ +jets background, opposite-sign to same-sign ratios for $W(\ell\nu)$ +jets (6%) and QCD (6%), and $t\bar{t}$ extrapolation (11%). The mass shape uncertainties arising from variations in tau, electron, and muon energy scales—3%, 2%, and 1%, respectively—are also included.

² τ_{had} stands for τ -leptons decaying hadronically

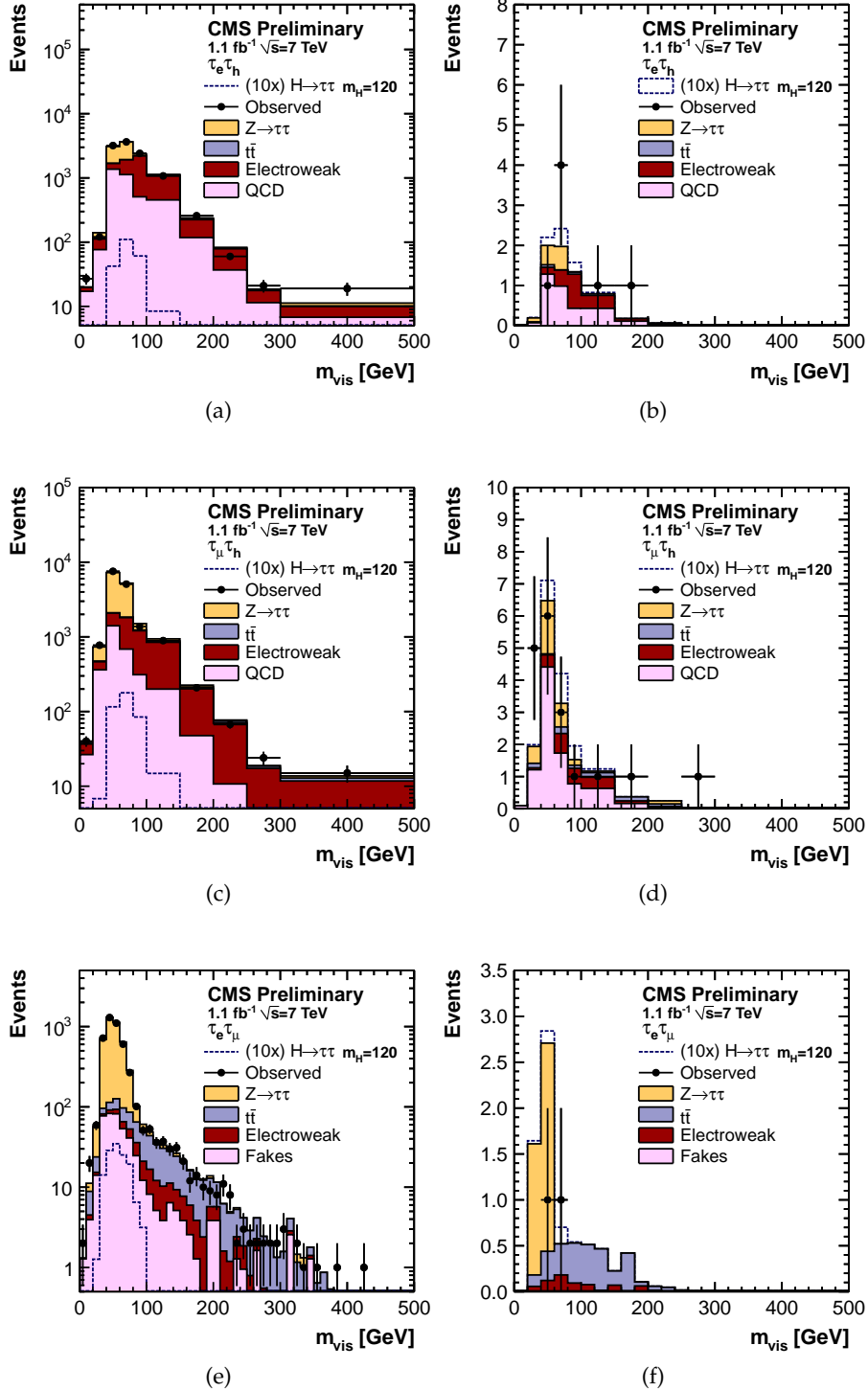


Figure 5: Input information from the $H \rightarrow \tau\tau$ analysis for a SM Higgs boson with $m_H = 120 \text{ GeV}/c^2$: visible mass distributions for (a) $e\tau_{had}$ and non-VBF selection, (b) $e\tau_{had}$ plus VBF selection, (c) $\mu\tau_{had}$ and non-VBF selection, (d) $\mu\tau_{had}$ plus VBF selection, (e) $e\mu$ and non-VBF selection, (f) $e\mu$ plus VBF selection. The observed events are shown with points, while the expected background and signal rates are represented by histograms. Signal is multiplied by a factor of 10, to be better visible. Normalizations for all backgrounds are obtained using data-driven techniques.

3.3 $H \rightarrow WW \rightarrow 2\ell 2\nu$ channel [7]

In this channel, we search for events with two oppositely charged leptons and large missing energy arising from neutrinos in W -decays. In addition to the angular separation between the leptons which distinguishes the scalar $H \rightarrow WW \rightarrow 2\ell 2\nu$ decay from the $WW \rightarrow 2\ell 2\nu$ background, we rely on the multivariate analysis (MVA) techniques that consolidate all discriminating information from multiple observables and their correlations into one final observable, called MVA-output. The search is based on the analysis of the MVA-output distributions.

Events are collected using single and di-lepton triggers. In the offline analysis of recorded data, we consider muons with $p_T > 10 \text{ GeV}/c$ and $|\eta| < 2.4$ and electrons with $p_T > 10 \text{ GeV}/c$ and $|\eta| < 2.5$. We require there to be two oppositely-charged, isolated leptons, in three final states: e^+e^- , $\mu^+\mu^-$, or $e^\pm\mu^\mp$. Both leptons are required to be isolated. Electrons originating from photon conversions are suppressed requiring no missing hits along their trajectory in the pixel detector and a low probability of the conversion vertex fit. Events with more than two high- p_T leptons are rejected in order to reduce the WZ and ZZ backgrounds.

To help suppress the $t\bar{t}$ background, events with additional soft muons are vetoed. We also veto events with b -tagged jets. Events with two same-flavor leptons forming an invariant mass within $\pm 15 \text{ GeV}/c^2$ around the pole Z -boson mass are rejected (Z -veto). To further suppress the Drell-Yan background, we require that the projection of the missing transverse energy onto the direction transverse to the nearest lepton must be greater than 40 (20) GeV for same-flavor (opposite-flavor) di-lepton events. We also veto events where the di-lepton system is found to approximately against a leading jet with $E_T > 15 \text{ GeV}$, i.e. events with $\Delta\phi_{\ell\ell, \text{jet}} > 165^\circ$.

Finally, events are classified by the presence of 0, 1, or 2 jets with $p_T > 30 \text{ GeV}/c$ and $|\eta| < 5.0$. The 0- and 1-jet bin categories are further split into same-flavor (SF) and opposite-flavor (OF) groups. Hence, the current analysis is based on 5 independent sub-channels.

To make maximal use of the event information, we have performed a multivariate analysis, here using a multivariate classifier based on the Boosted Decision Tree (BDT) technique for the zero-jet and one-jet bins. The following variables are used in MVA training: flavor of leptons, the transverse momenta of the harder and the softer leptons; the di-lepton mass; the distance between the two selected leptons in $\Delta\phi$, $\Delta\eta$, ΔR ; and three transverse masses built from pairing the missing transverse energy separately with the hard lepton, the soft lepton, and the di-lepton system. The training is performed using Monte Carlo Higgs events as a signal and Monte Carlo W^+W^- continuum as background.

For the two-jet bin, the analysis is based on the cut-and-count approach. In addition to the basic selection described earlier, we require the two jets have VBF-like kinematics: exactly 2 jets with $m_{jj} > 450 \text{ GeV}/c^2$ and $|\Delta\eta_{jj}| > 3.5$.

The BDT-classifier outputs for $m_H = 160 \text{ GeV}/c^2$ analysis in the zero-jet and one-jet bins, together the $|\Delta\eta_{jj}|$ distribution for the 2-jet bin, are shown in Figure 6 and 7.

After all selection cuts applied, the main backgrounds are: W^+W^- continuum, $t\bar{t}$, Drell-Yan, W +jets, and WZ/ZZ . All the main backgrounds are evaluated using the following data-driven techniques.

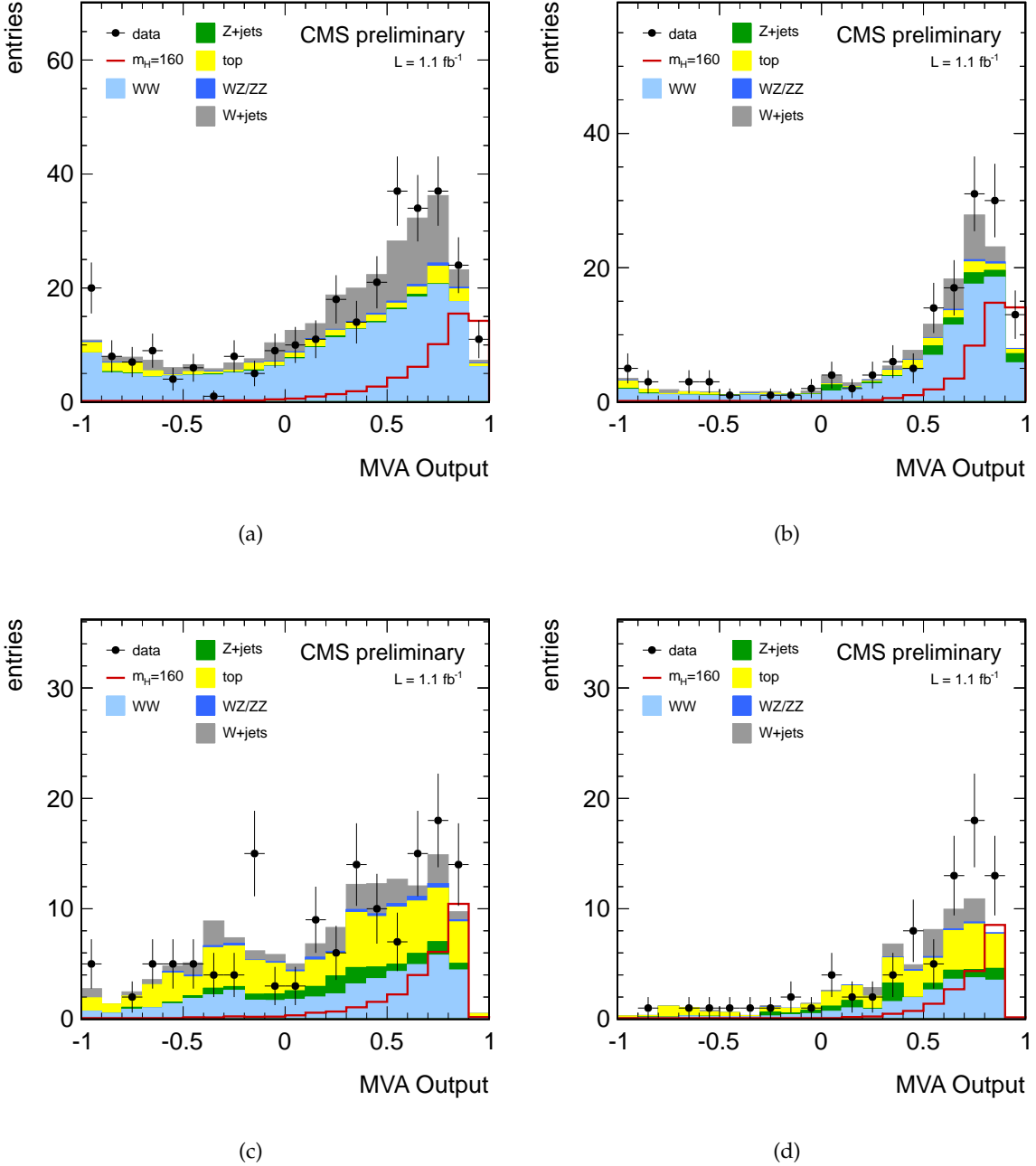
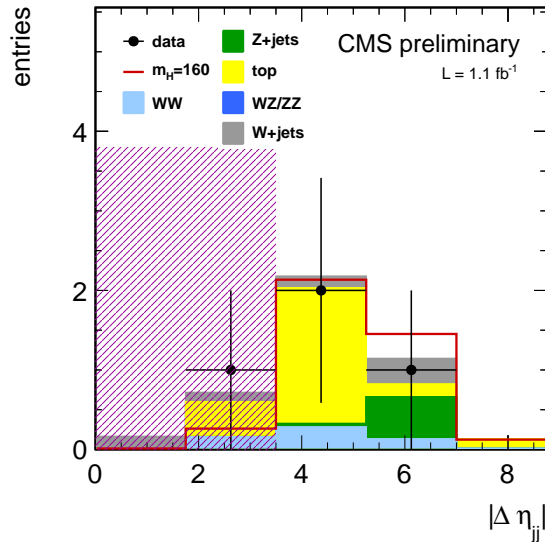


Figure 6: Input information from the $H \rightarrow WW \rightarrow 2\ell 2\nu$ analysis for a SM Higgs boson with $m_H = 160 \text{ GeV}/c^2$: (a) MVA output distributions for $e\mu$ events with no jets, (b) MVA output distributions for ee and $\mu\mu$ events with no jets, (c) MVA output distributions for $e\mu$ events with 1 jet, (d) MVA output distributions for ee and $\mu\mu$ events with 1 jet. The observed data (points) and expected background and signal rates (histograms) are shown. Normalizations for the WW , $t\bar{t}$, W +jets, and Drell-Yan background predictions are obtained using data-driven techniques.

The $t\bar{t}$ background is estimated by extrapolation from the observed number of events with the b -tagging cut inverted. The Drell-Yan background measurement is based on extrapolation from the observed number of e^+e^- , $\mu^+\mu^-$ events with the Z -veto cut inverted. The background W +jets and QCD multi-jet events is derived from measuring the number of events with one lepton passing a loose cut on isolation. The probabilities for such loosely-isolated fake leptons to pass tight isolation cut are measured in data using multi-jets and γ -jet events.

The non-resonant WW contribution for low mass signal region, $m_H < 200 \text{ GeV}/c^2$, is estimated using events with a di-lepton mass larger than $100 \text{ GeV}/c^2$, where there is a negligible contamination from the Higgs boson signal. For larger Higgs boson masses there is a large overlap between the non-resonant WW background and a Higgs boson signal and we thus use simulation.

The largest uncertainties on the signal yield include theoretical errors on total cross sections (5-15%), acceptance for exclusive 0/1/2-jet final states (7-20%), and luminosity (6%). The largest background systematic errors come from statistical uncertainties in the number of events observed in the control samples (20-60%), Monte Carlo statistical errors limiting the accuracy with which we can validate the data-driven techniques (10-20%), and from application of the lepton fake rate estimation to W +jets control sample .



(a)

Figure 7: Input information from the $H \rightarrow WW \rightarrow 2\ell 2\nu$ analysis for a SM Higgs boson with $m_H = 160 \text{ GeV}/c^2$: $|\Delta\eta_{jj}|$ distributions for 2ℓ events with 2 jets (events with low values of $|\Delta\eta|$, hatched out in the plot, are not used). The observed data (points) and expected background and signal rates (histograms) are shown.

3.4 $H \rightarrow ZZ \rightarrow 4\ell$ channel [8]

In this channel, we search for a narrow resonance peaked over the continuum four-lepton mass $m_{4\ell}$ distribution. The number of observed events is very low and we use the unbinned approach. The analysis is performed in three sub-channels: $4e$, 4μ , $2e2\mu$.

Events used in the analysis have been collected by di-lepton triggers at low and high luminosities, respectively. To be considered in the offline analysis, electrons are required to have $p_T > 7$ GeV/ c and $|\eta| < 2.5$ and muons must have $p_T > 5$ GeV/ c and $|\eta| < 2.4$. Also, such leptons must be isolated in the tracking and calorimeter detectors and must not have large significance of the 3D impact parameters with respect to the common vertex. In events with four or more leptons, we ask for at least one pair of same-flavor opposite-charge di-leptons satisfying the following cuts: $p_T^{max} > 20$ GeV/ c , $p_T^{min} > 10$ GeV/ c , $60 < m_{\ell\ell} < 120$ GeV/ c^2 . If more than one pair satisfies this requirement, the one with the invariant mass closest to the Z-boson mass is picked. The second pair of same-flavor, opposite-charge leptons must form an invariant mass $20 < m_{\ell\ell} < 120$ GeV/ c^2 . If more than one four-lepton combination satisfies all the criteria, then the one with the highest p_T leptons is chosen. Four leptons selected in such a process form a ZZ event candidate with a mass $m_{4\ell}$.

Fig. 8 shows observed events as well as parametric density functions for the expected backgrounds and signal for a Higgs boson mass of $m_H = 300$ GeV/ c^2 .

The signal shape $f_S(m_{4\ell})$ is constructed as the Breit-Wigner function convoluted with the detector four-lepton mass resolution emulated with the crystal ball function. Default parameters are derived from fitting simulated Higgs events, which were generated using the next-to-leading-order (NLO) matrix-element generator POWHEG [23] interfaced to PYTHIA [24] for parton showering and passed through the full detector simulation.

The dominant irreducible background is the electroweak ZZ-production. The mass shape for this background is known at NLO and further corrected to include the contribution of $gg \rightarrow ZZ \rightarrow 4\ell$. Both the NLO $m_{4\ell}$ shape and an additional gg -correction were evaluated with MCFM [27]. To reduce systematic errors associated with luminosity and lepton reconstruction/identification efficiencies, the overall event yield of the ZZ-background is obtained by scaling the observed numbers of Z-events in the $2e$ - and 2μ -channels by the theoretical ratio of ZZ of Z cross sections. The reducible backgrounds $Z + jets$ (including heavy flavor jets) and $t\bar{t}$ are evaluated from the data, relying on the inversion of the isolation and impact parameter cuts—their contribution is estimated to be almost negligible.

The main sources of systematic errors on signal and irreducible backgrounds are due to theoretical uncertainties on their cross sections: 6% (QCD scales) and 8% (PDF) for Higgs and 7% (combined) for ZZ. For Higgs boson masses $m_H > 300$ GeV/ c^2 , theoretical uncertainties on the virtual Higgs mass lineshape may become large; however, for a lack of a model for such uncertainties, they are not included in these preliminary results. Trigger, lepton reconstruction, and isolation cut efficiencies for prompt leptons are derived from data using $Z \rightarrow ee$ and $Z \rightarrow \mu\mu$ events (tag-and-probe method) with the net uncertainty on the event yields of about 1-3%.

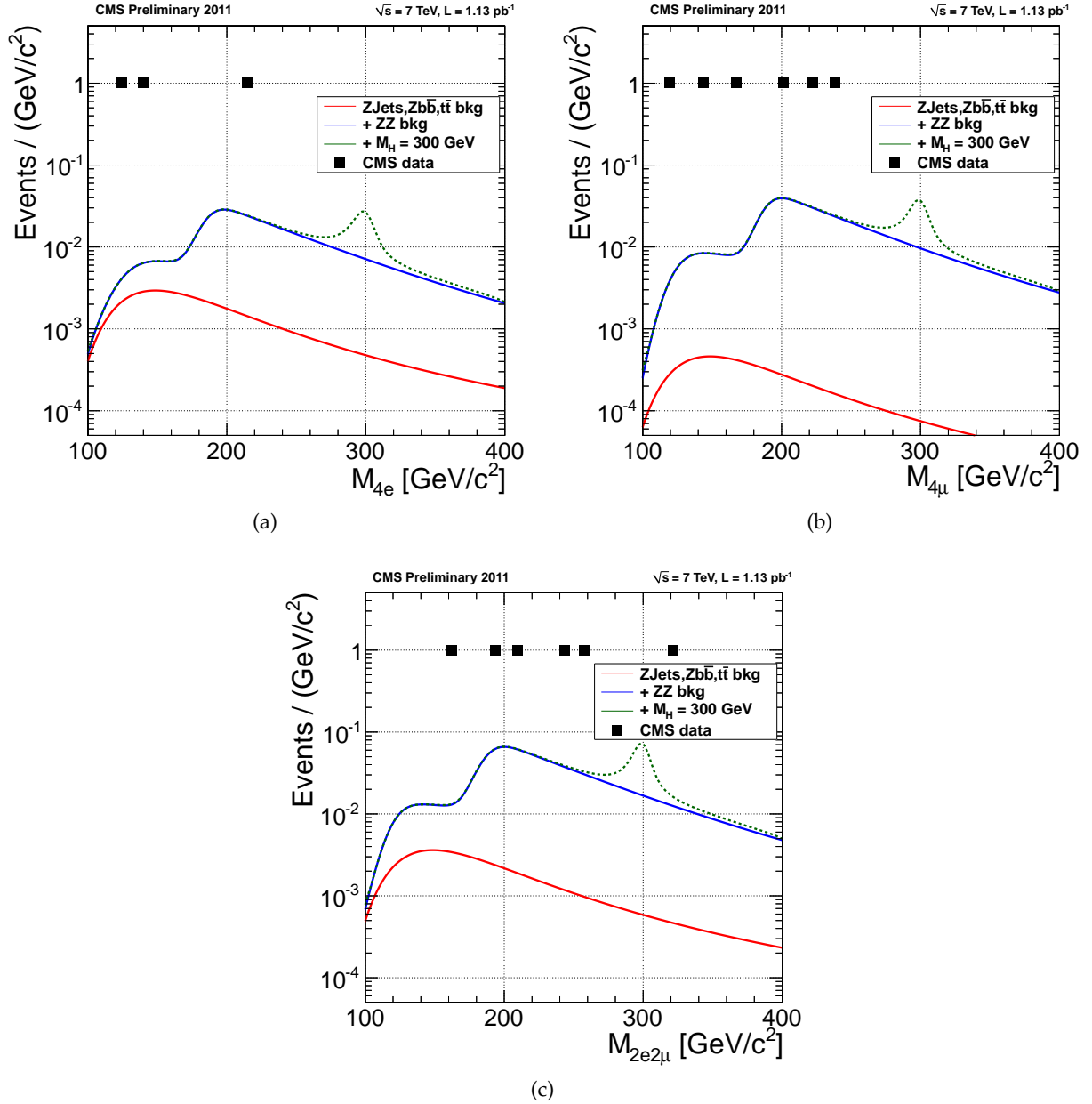


Figure 8: Input information from the $H \rightarrow ZZ \rightarrow 4\ell$ analysis for a SM Higgs boson with $m_H = 300 \text{ GeV}/c^2$: $m_{4\ell}$ mass distributions for (a) $4e$, (b) 4μ , and (c) $2e2\mu$ final states. The observed events are indicated by square symbols. The curves show parametric density functions for the expected background and signal rates. Normalization for reducible backgrounds is obtained using data-driven techniques.

3.5 $H \rightarrow ZZ \rightarrow 2\ell 2\nu$ channel [9]

In this channel, the search is performed using a cut-and-count approach and two sub-channels: $2e2\nu, 2\mu 2\nu$.

Events are selected using double-lepton triggers. The two leptons are required to pass all prompt lepton identification cuts (basic id, isolation, impact parameter), satisfy kinematic cuts and form an invariant mass in a $\pm 15 \text{ GeV}/c^2$ mass window around m_Z , and have $p_T(\ell\ell) > 25 \text{ GeV}/c$. Furthermore, cuts on the missing transverse energy MET , M_T (defined in footnote ³), and $\Delta\phi(MET, Jet)$ are applied to suppress a huge reducible background of $Z + jets$. MET , M_T , and $d\phi(MET, Jet)$ cuts depend on the Higgs boson mass being searched for. To help suppress the $t\bar{t}$ and single-top -backgrounds, events with b-tagged jets are vetoed. Figure 9 shows the final M_T distributions for the two sub-channels before the M_T cut is applied.

The ZZ and WZ backgrounds are taken from Monte Carlo simulation. The WZ background cross section is calculated at NLO. The ZZ background is a combination of NLO ZZ and $gg \rightarrow ZZ$, known at LO.

The Z +jets background has a very large cross section and is suppressed by the analysis cuts with an efficiency $O(10^{-5})$. To estimate the remaining rate of Z +jets events, we rely on the data-driven technique taking advantage that $Z(\ell\ell)$ +jets and γ +jets are very closely related, while the latter has a much higher observable event yield.

The *non-resonant* backgrounds, i.e. those without Z -boson (mostly, $t\bar{t}$ and WW), are also derived from data, taking advantage that non-resonant backgrounds, in addition to e^+e^- and $\mu^+\mu^-$, also, give $e^\pm\mu^\mp$ events.

The main sources of systematic errors on signal and irreducible backgrounds are due to theoretical uncertainties on their cross sections (up to 15% for Higgs, 7.8% for $qq \rightarrow ZZ$ and 20% for $gg \rightarrow ZZ$). The main uncertainties for backgrounds are coming from the methods used to measure the backgrounds from data - the channel is characterized by tight cuts and little populated phase space, therefore methods as of now are limited by statistics available (with typical uncertainty 50%).

³ M_T is defined as follows: $M_T^2 = (\sqrt{P_{TZ}^2 + M_Z^2} + \sqrt{MET^2 + M_Z^2})^2 - (P_{TZ} + M\vec{E}T)^2$.

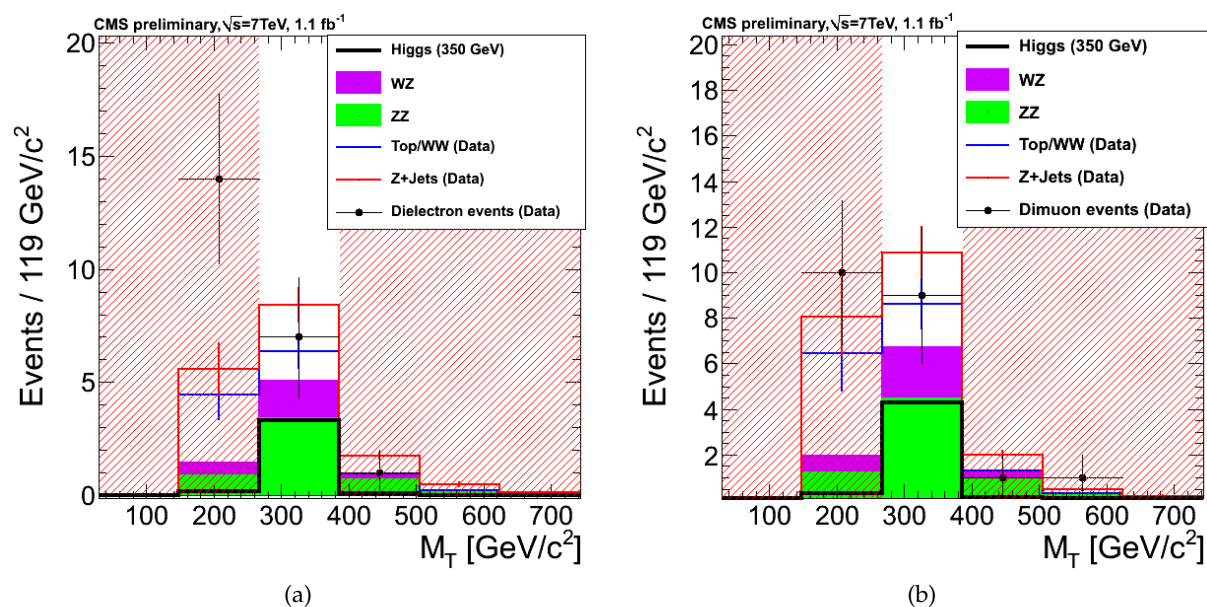


Figure 9: M_T distributions for (a) $Z_{ee} + MET$ and (b) $Z_{\mu\mu} + MET$ events with cuts optimized for a search of the standard model Higgs boson with mass $m_H = 350\text{ GeV}/c^2$. The observed data (points) and expected background and signal rates (histograms) are shown. Some of the backgrounds are obtained using data-driven techniques as indicated on the plots. Only the bin not covered by the hatched area was used in the statistical analysis of data for the given Higgs boson mass.

3.6 $H \rightarrow ZZ \rightarrow 2\ell 2q$ channel [10]

The Higgs boson search in the channel $H \rightarrow ZZ \rightarrow 2\ell 2q$ proceeds by searching for a peak in the invariant mass of the dilepton plus dijet system m_{ZZ} . The width of the peak is affected by the jet energy resolution and is improved by constraining the dijet invariant mass to the Z boson mass.

The main sources of background are $Z + jets$ and a small contribution of $t\bar{t}$ and electroweak diboson production. Leptons are required to be isolated and to pass quality requirements. The leading lepton must have $p_T > 40$ GeV/ c and the other one $p_T > 20$ GeV/ c . All jets are required to have $p_T > 30$ GeV/ c . In order to further reduce the amount of background, requirements on dijet and dilepton invariant masses are applied: $75 < m_{jj} < 105$ GeV/ c^2 and $70 < m_{\ell\ell} < 110$ GeV/ c^2 . Events are categorized in different exclusive channels according to the lepton flavour ($2e2q$ and $2\mu 2q$) and according to the number of b -tagged jets (zero, one, or two b -tagged jets). Further background rejection is achieved by exploiting the different angular distribution of Higgs boson signal with respect to background and applying a quark-gluon discriminator in the category with no b -tagged jets, which is the most affected by $Z + jets$ background. To help suppress $t\bar{t}$ background in the category with 2 b -tagged jets, a cut missing transverse energy significance is also used.

The statistical analysis is based on the m_{ZZ} distribution. The background shape and normalization are determined from data using the m_{ZZ} distribution in the sidebands obtained by inverting the m_{jj} requirement using an unbinned maximum likelihood fit. The signal shape is described by a relativistic Breit-Wigner convoluted with a Crystal-Ball function determined from simulation. The signal reconstruction efficiency and the resolution function are parameterized as a function of the hypothetical Higgs boson mass.

Figure 10 shows the observed data, the expected background, as derived from an independent data control sample, and an example of the expected signal.

The main sources of systematic uncertainty affecting the signal yield are the uncertainties on the total cross section and branching ratio, $\sim 17\%$, and the integrated luminosity, $\sim 6\%$. The uncertainty on b -tag efficiency can vary from 1% to 20% depending on the category. Effects from lepton energy scale, muon and electron reconstruction efficiency, jet resolution and efficiency, pile-up, quark-gluon discrimination, E_T^{miss} and production mechanism are considered as well.

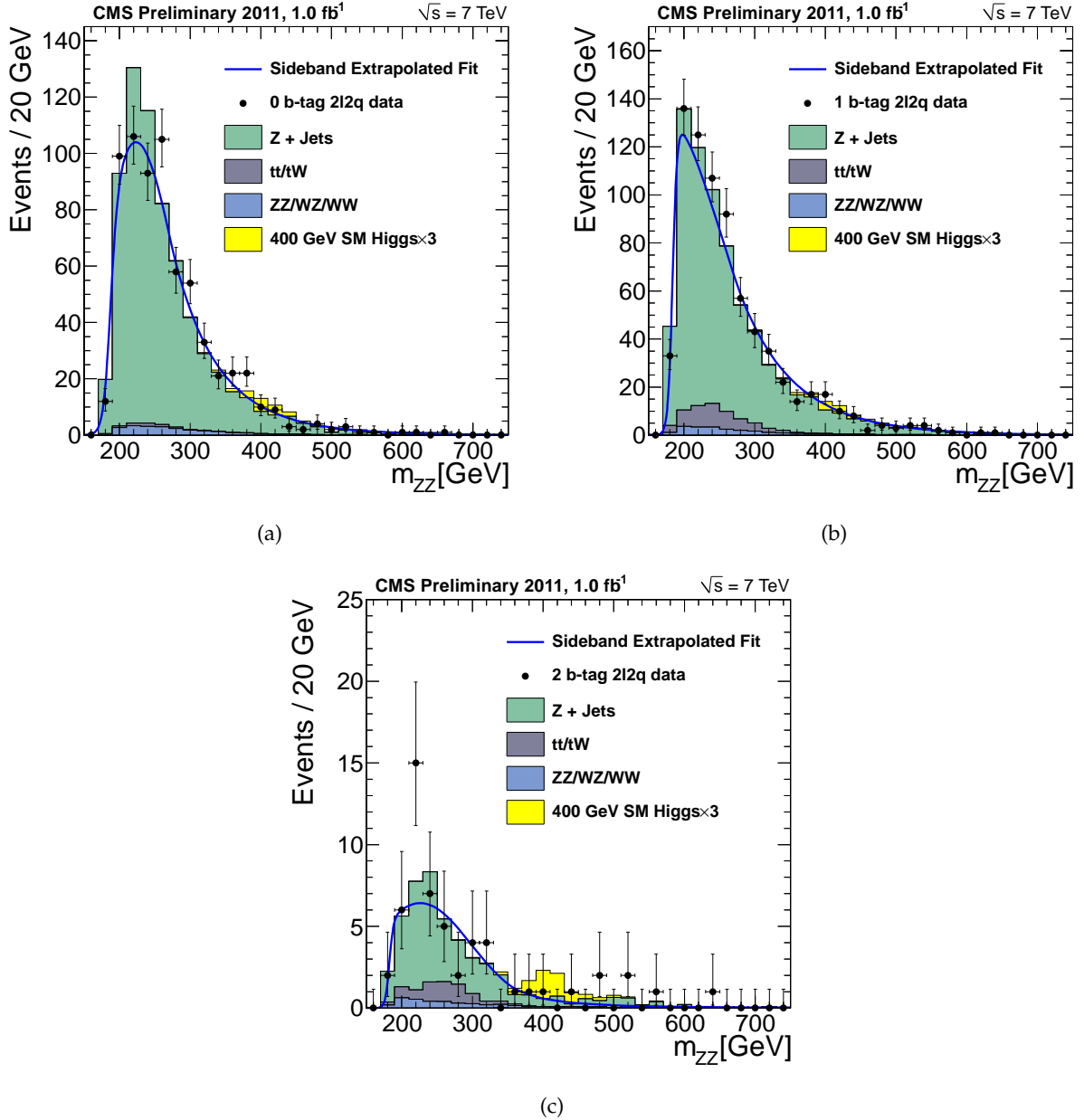


Figure 10: Binned $m_{2\ell 2j}$ distributions for: (a) $2\ell+2j$, with 0 b-tags, (b) $2\ell+2j$, with 1 b-tag, (c) $2\ell+2j$, with 2 b-tag. The $2e$ and 2μ final states are combined together here, but in the overall statistical analysis they are treated separately. The line corresponds to the background model, whose shape and normalization are derived from independent control samples. Monte Carlo generated background distributions are shown only for comparison,—they are not used directly in the statistical analysis. The expected SM Higgs boson signal, multiplied by a factor of 3, for $m_H = 400$ GeV/ c^2 is also shown. Although the data are shown as binned distributions, the actual analysis is carried out in the unbinned manner.

4 Higgs search results

4.1 Summary and discussion of results obtained in the individual analyses

None of the searches performed in the six channels entering the overall combination shows a significant excess of events. Limits on the signal strength modifier $\mu = \sigma/\sigma_{SM}$, as obtained individually in each of these searches are shown in left panels of Figs. 11- 16. As to be expected, some fluctuations are observed. The corresponding p -values and best-fit $\hat{\mu}$ values are shown in the right hand panels of Figs. 11-16, and discussed further below.

The left hand plots in Figs. 11-16 show the limits on the signal strength modifier, with the solid lines denoting the experimentally observed limits and the dashed lines the median expected limits for the background-only hypothesis. The solid color bands indicate the possible variation in the expected limit in the background-only hypothesis, given the current statistical and systematic errors. The green (yellow) bands are expected to contain 68% (95%) of all excursions of the expected limit.

The lower panel on the right hand side of Figs. 11-16 shows the observed p -values, indicating how incompatible an observed excess is with the background-only hypothesis. However, p -values by themselves do not provide any information on whether an observed excess is consistent with the SM Higgs boson hypothesis or not. The best fit value of $\hat{\mu}$ indicates what signal strength would be most consistent with an observed excess, and is shown in the upper right panels with a solid line. The light blue band indicates the $\pm 1\sigma$ range is obtained in the fit.

The expected limits for the $H \rightarrow \gamma\gamma$ channel are fairly flat in the chosen range, but then deteriorate for $m_H < 110 \text{ GeV}/c^2$ and $m_H > 140 \text{ GeV}/c^2$ mostly due to the decrease in the branching ratio $\text{BR}(H \rightarrow \gamma\gamma)$ outside the 110-140 GeV/c^2 mass range and larger background at low masses. The observed limits exhibit some fluctuations with a correlation length characteristic of the average $\gamma\gamma$ mass resolution. The p -value of the largest excess is just below 2σ -level. Taking into account the look-elsewhere effect, evaluated by generating pseudo-data for the background-only hypothesis, the chance of observing a maximum excess as large as seen in the data is about 60%, giving a trials factor $\text{O}(20)$.

The $H \rightarrow \tau\tau$ channel is rather featureless, which stems from the $\tau\tau$ mass resolution being comparable to the explored range of Higgs boson masses. The degradation in the expected limit at higher masses results from the decrease in the branching ratio $\text{BR}(H \rightarrow \tau\tau)$ and the decreasing signal cross section. The observed limits are consistent with the expectation.

The $H \rightarrow WW \rightarrow 2\ell 2\nu$ channel has a pronounced strong sensitivity (low expected limit on μ) around $m_H = 160 \text{ GeV}/c^2$, where $\text{BR}(H \rightarrow WW) \sim 100\%$. At lower masses, the branching ratio falls very quickly. At higher masses, while the branching ratio remains fairly high, the signal cross section falls and the expected limits deteriorate. The observed limits in the low mass range below $180 \text{ GeV}/c^2$ show a broad $\sim 2\sigma$ upward deviation. This observed excess weakens the limits that we set in this mass range. Since in this analysis one does not have a direct measure of the Higgs boson mass, the correlation length for excursions of the observed limit curve is large and estimated to be $\pm 30 \text{ GeV}/c^2$ in the low mass range by injecting signal Monte Carlo events into pseudo-data, which resulted in broad excesses over a 50-80 GeV/c^2 mass range. Fluctuations of the number of background events would also appear as similarly broad “low frequency” excursions of the observed limit curve away from the median expected. The overall look-elsewhere effect is small. For the full mass range used in the search, the trial factor is estimated to be of the order of three. The values of $\hat{\mu}$ well above (below) $\hat{\mu} = 1$ in the $< 120 \text{ GeV}/c^2$ ($> 140 \text{ GeV}/c^2$) range indicate that the excess is too large (too low) for the SM Higgs boson. More data will confirm whether the observed excess is a statistical background

fluctuation or not.

The $H \rightarrow ZZ \rightarrow 4\ell$ channel has a very characteristic structure in the expected limits that mirrors the dependence of the branching ratio $\text{BR}(H \rightarrow ZZ)$ on the Higgs boson mass. The worsening limits at high masses come from the decreasing signal cross section. The reduced sensitivity around $m_H = 160 \text{ GeV}/c^2$ and for low masses comes from the very small $H \rightarrow ZZ$ branching ratio in these regions. The overall background rate, dominated by the electroweak ZZ di-boson production, is very low. The four-lepton mass resolution is very good. Therefore, the structure in the observed limits basically follows the distribution of the observed events (see Fig. 8). The total number of events with $m_{4\ell} > 100 \text{ GeV}/c^2$ is 15, while 14.4 ± 0.6 events are expected from standard model background processes. Six of the events are below the kinematic threshold of two on-shell Z s ($m_H < 180 \text{ GeV}/c^2$), which is higher than the expected 1.9 ± 0.1 . These six events form roughly three pairs around 120, 140, and 160 GeV/c^2 , rulling out a common narrow source such as a SM-like signal. The $\hat{\mu}$ scan shows that the two dips of p -value around $m_H \sim 120$ and 160 GeV/c^2 would require a much stronger signal than the SM Higgs boson, while the two events around 140 GeV/c^2 are not inconsistent with the SM Higgs. The look-elsewhere effect in this analysis is of the order of $\mathcal{O}(100)$ as estimated by repeatedly generating pseudo-data for the background-only hypothesis and performing pseudo-searches for a signal [28]. The overall trial factor is approximately driven by the mass range used in the analysis and the width of the resonant peak being searched for. The minimal p -value observed ~ 0.01 , is thus not unlikely with such a large trial factor. Overall, the look-elsewhere effect washes out the level of significance of the dips we see in the p -value scan, and, currently, we set limits on the SM Higgs boson signal strength modifier μ .

The expected limits for $H \rightarrow ZZ \rightarrow 2\ell 2\nu$ and $H \rightarrow ZZ \rightarrow 2\ell 2q$ channels have a typical concave structure. As one moves toward the lower masses, the Z +jets background quickly overwhelms a potential signal. Cuts optimized for a higher Higgs boson mass allow one to suppress this formidable background, but eventually the signal cross section becomes too small and limits worsen. The observed limits in these two channels fluctuate, as expected, with an absolute scale and “correlation length” consistent with expectations.

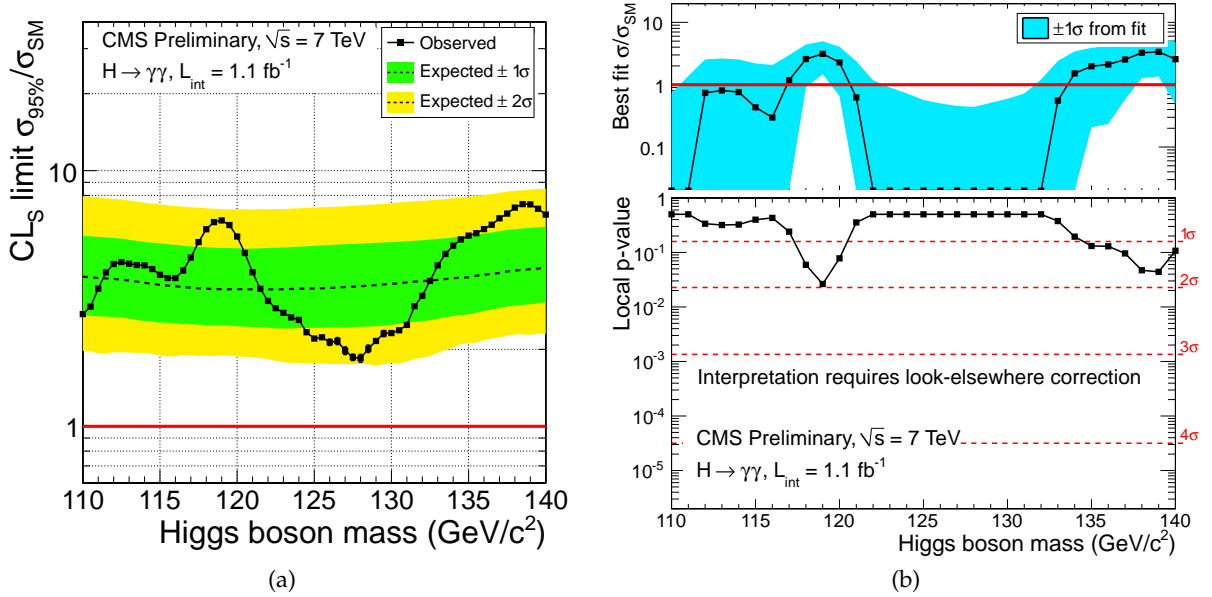


Figure 11: Search results in the $H \rightarrow \gamma\gamma$ analysis. (Left) Limits on the signal strength modifier $\mu = \sigma/\sigma_{SM}$. (Right) p -values characterizing how unlikely the observed “local” excesses are (bottom sub-panel) and what best-fit signal strength modifier $\hat{\mu}$ they would correspond to (top sub-panel). See the discussion of the results in the text.

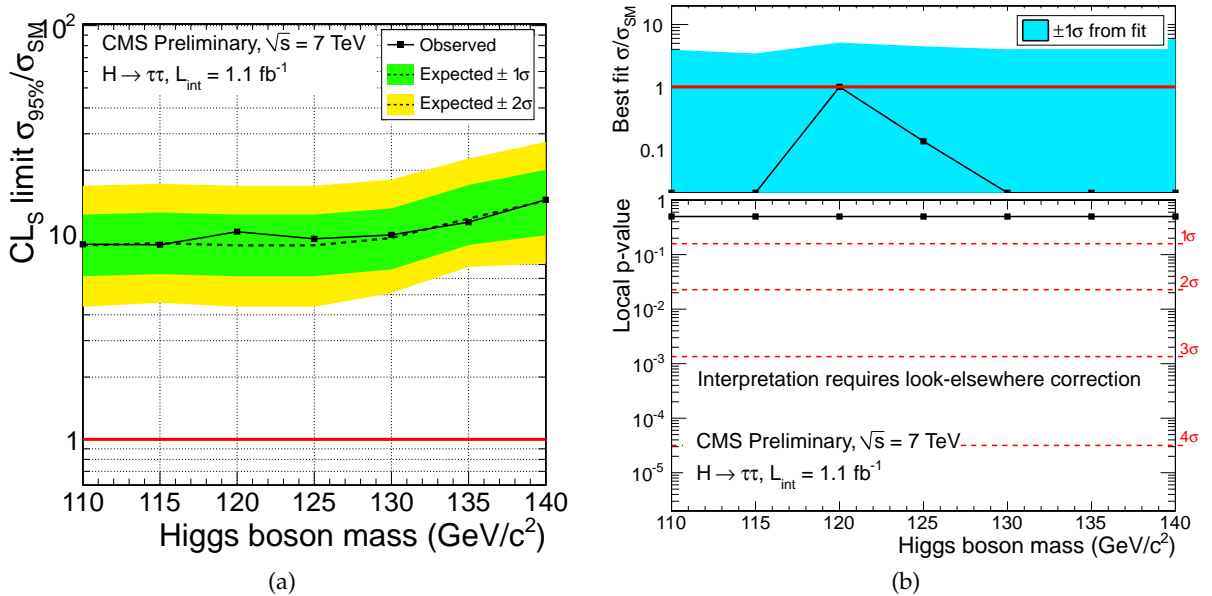


Figure 12: Search results in the $H \rightarrow \tau\tau$ analysis. (Left) Limits on the signal strength modifier $\mu = \sigma/\sigma_{SM}$. (Right) p -values characterizing how unlikely the observed “local” excesses are (bottom sub-panel) and what best-fit signal strength modifier $\hat{\mu}$ they would correspond to (top sub-panel). See the discussion of the results in the text.

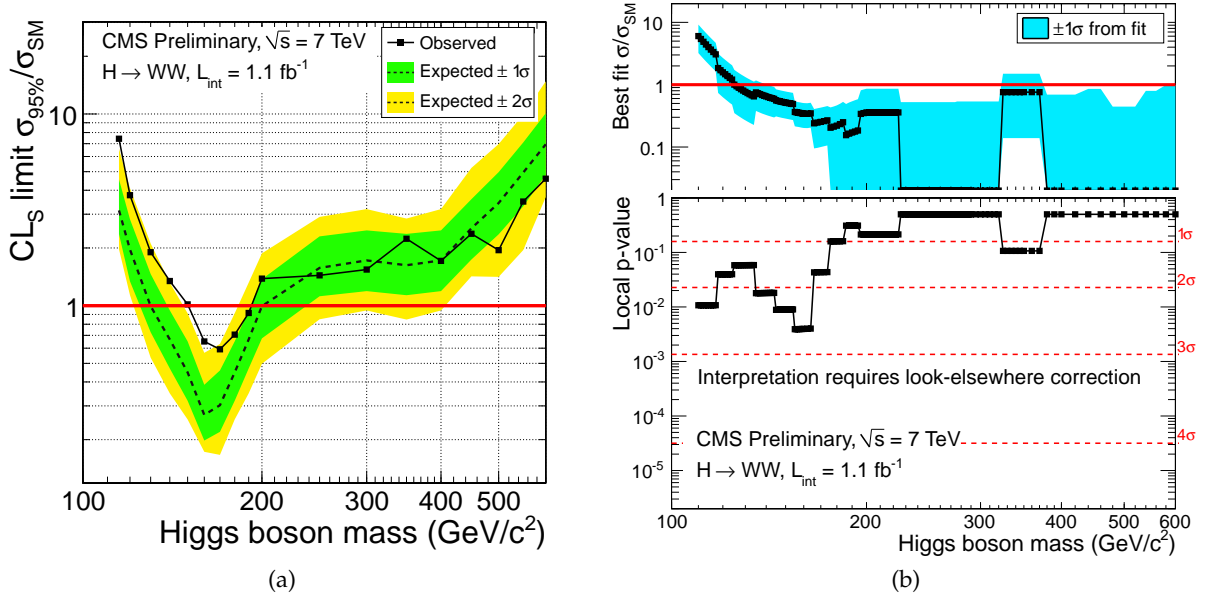


Figure 13: Search results in the $H \rightarrow WW \rightarrow 2\ell 2\nu$ analysis. (Left) Limits on the signal strength modifier $\mu = \sigma/\sigma_{SM}$. (Right) p -values characterizing how unlikely the observed “local” excesses are (bottom sub-panel) and what best-fit signal strength modifier $\hat{\mu}$ they would correspond to (top sub-panel). See the discussion of the results in the text.

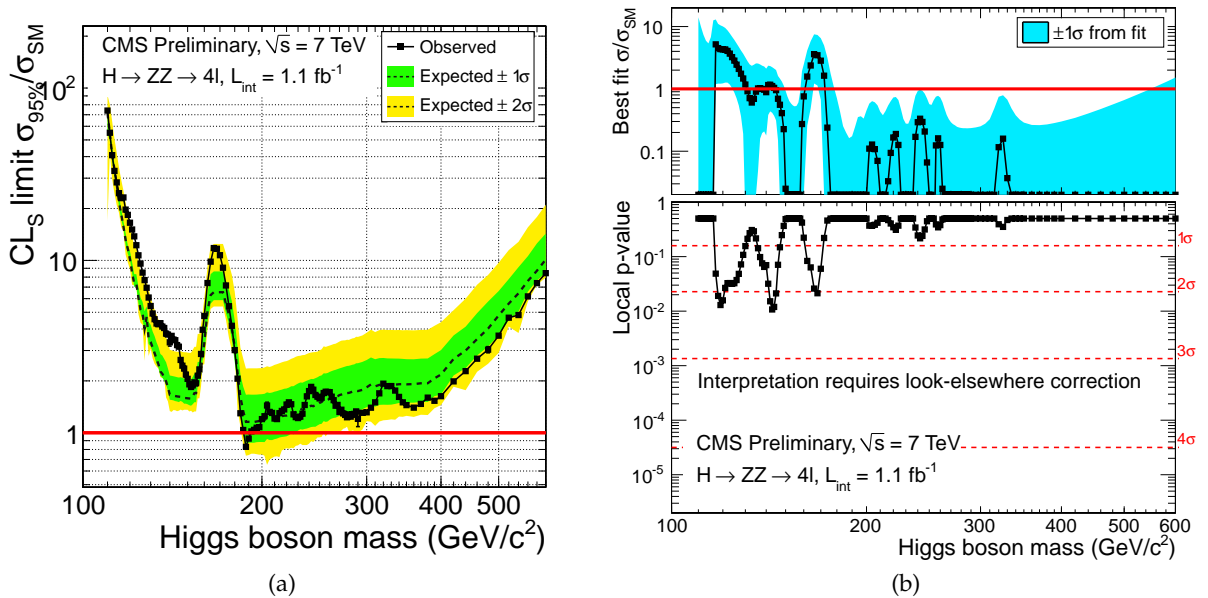


Figure 14: Search results in the $H \rightarrow ZZ \rightarrow 4\ell$ analysis. (Left) Limits on the signal strength modifier $\mu = \sigma/\sigma_{SM}$. (Right) p -values characterizing how unlikely the observed “local” excesses are (bottom sub-panel) and what best-fit signal strength modifier $\hat{\mu}$ they would correspond to (top sub-panel). See the discussion of the results in the text.

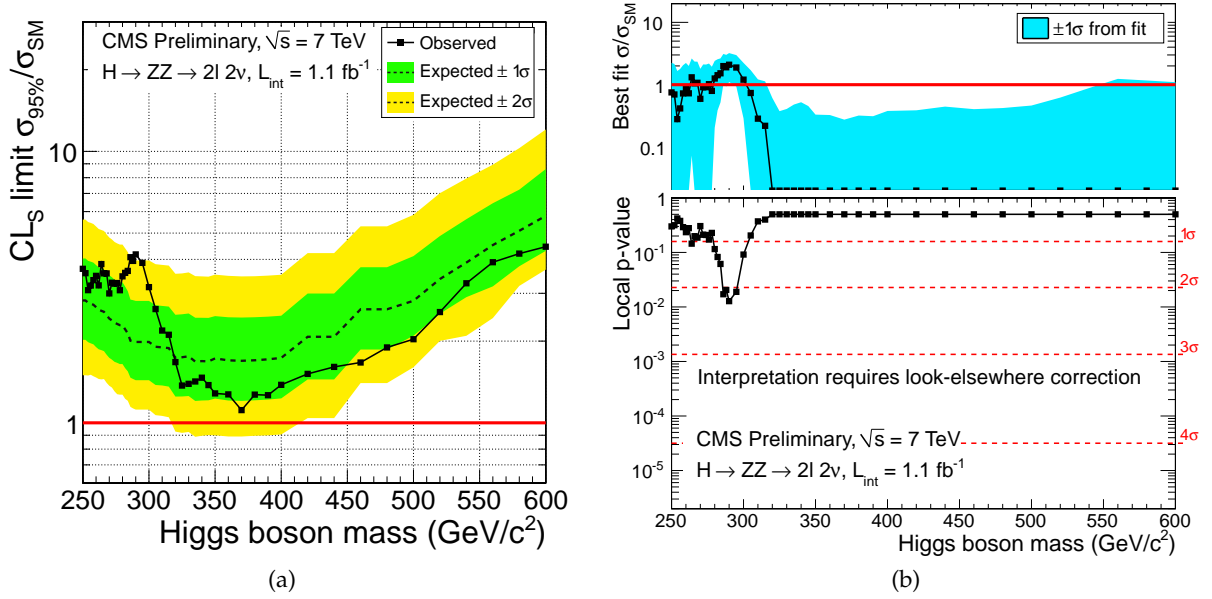


Figure 15: Search results in the $H \rightarrow ZZ \rightarrow 2\ell 2\nu$ analysis. (Left) Limits on the signal strength modifier $\mu = \sigma/\sigma_{SM}$. (Right) p -values characterizing how unlikely the observed “local” excesses are (bottom sub-panel) and what best-fit signal strength modifier $\hat{\mu}$ they would correspond to (top sub-panel). See the discussion of the results in the text.

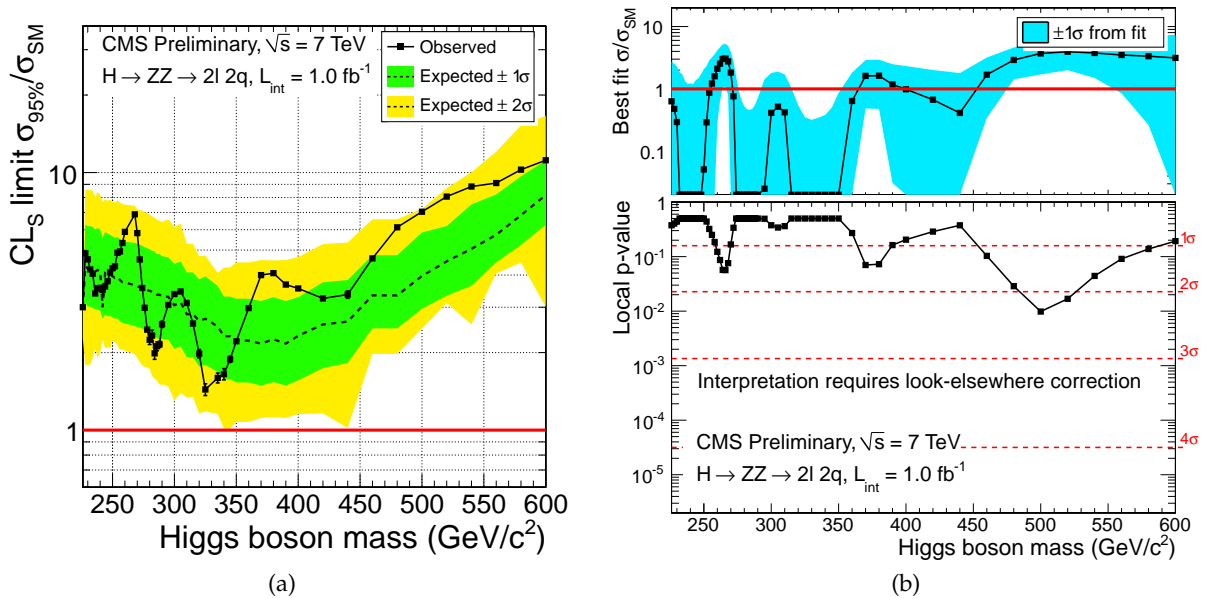


Figure 16: Search results in the $H \rightarrow ZZ \rightarrow 2\ell 2q$ analysis. (Left) Limits on the signal strength modifier $\mu = \sigma/\sigma_{SM}$. (Right) p -values characterizing how unlikely the observed “local” excesses are (bottom sub-panel) and what best-fit signal strength modifier $\hat{\mu}$ they would correspond to (top sub-panel). See the discussion of the results in the text.

4.2 Combination results: search for the SM Higgs boson

The results of combining all six analyses discussed in the previous section into one grand search for the SM Higgs boson are presented in Figs. 17, 18, and 19.

Figure 17 shows the CL_s value for the SM Higgs boson as a function of its mass. The observed values are shown by the solid line. The dashed line indicates the median expected value of CL_s , while the green/yellow bands indicate the $\pm 1\sigma$ (68%) and $\pm 2\sigma$ (95%) ranges in which the observed results are expected to reside for the *background-only* hypothesis. We exclude the SM Higgs boson at 95% C.L. in the two mass ranges 149-206 and 300-440 GeV/c^2 and a number of short segments in between. This substantially extends the exclusion limits established by LEP and Tevatron to date. The expected exclusion, in the absence of a signal, is from 127-420 GeV/c^2 . The difference between the observed and expected limits is consistent with statistical fluctuations. At the 90% C.L., the observed exclusion range is from 145-480 GeV/c^2 , without interruptions.

The observed CL_s values are about 2σ larger than expectation in the mass range of 130-170 GeV/c^2 , which is largely driven by the broad excess in the $H \rightarrow WW \rightarrow 2\ell 2\nu$ channel discussed in the previous section. Therefore, the observed exclusion in this mass range is not as strong as expected. At high masses, on the other hand, we see somewhat fewer events than expected, but still consistent with the expected level of statistical fluctuations. Such downward fluctuations make observed limits stronger than expected. The noticeable step-like structure of both observed and expected limits is a direct consequence of the $H \rightarrow WW \rightarrow 2\ell 2\nu$ analysis strategy, where the search is performed in small ranges of Higgs boson masses using an MVA technique, with independent trainings for each mass range. Therefore, discrete transitions from one mass range to the next cause abrupt changes in both observed and expected limits. The smoother fluctuations up and down are manifestations of the excesses / deficits seen in the other channels.

The combined 95% C.L. upper limits on the ratio of the excluded to the standard model cross sections $\mu^{95\%CL}$ as a function of the Higgs boson mass are presented in Fig. 18. This plot shows by what factor the SM Higgs boson cross section must be scaled to be excluded at 95% C.L. The exclusion range for the SM Higgs boson ($\mu = 1$) is identical to that shown in Fig. 17. Filled points show the observed CL_s -based limits. Open symbols are the limits obtained with the Bayesian approach. Although the two methodologies need not give identical results, the observed self-consistency of limits obtained with the two very different techniques is certainly reassuring. The CL_s and Bayesian limits on μ are remarkably consistent for all mass points in the scan; the relative differences are $0.3 \pm 4.7\%$. Naturally, the plots in Figs. 17 and 18 exhibit the same structure as they are basically different “representations” of intrinsically the same information.

Figure 19 shows the observed limits in the six individual analyses and their combination. At high masses, the combination of the four analyses considerably improves the observed exclusion over the results obtained in each analysis separately. At very low mass, at and just above $m_H = 110 \text{ GeV}/c^2$, the combination gives a less stringent limit than the results obtained in the $H \rightarrow \gamma\gamma$ analysis. This is due to an excess seen in the $H \rightarrow WW \rightarrow 2\ell 2\nu$ analysis.

Figures 20 and 21 show a scan of the observed combined \tilde{p} -value as given by Eq. (9) vs. Higgs boson mass m_H . This scan characterizes how unlikely the upward departures in the observed values of the test statistic q_0^{obs} approximately are ⁴ One can see that the p -value curve dips

⁴It is important to mention that the combined p -value cannot be evaluated from p -values as obtained for the individual channels for two main reasons. First, the best-fit values of $\hat{\mu}$ in different channels may be very different

downward over a broad range of low masses, driven by the excess seen in the WW -analysis, with three narrower features corresponding to the $ZZ \rightarrow 4\ell$ events and the modest excess seen in the $H \rightarrow \gamma\gamma$ channel.

However, one has to bear in mind that the look-elsewhere effect has not yet been evaluated for this combination. Individual channels going into the combination have their trials factors ranging from $O(1)$ - $O(100)$, as discussed earlier. The overall trials factor in the combination depends strongly on the relative sensitivities of individual channels. Therefore, the actual significance of the observed low p -values is smaller, potentially much smaller, than the “local” p -values may imply.

As discussed before, while a small p -value does characterize the chance for an upward fluctuation of the background to be as large as observed, it does not tell us whether such an excess is actually consistent with the signal or not. Therefore, in addition, we show the best-fit $\hat{\mu}$ value that represents the factor by which the SM Higgs boson cross section has to be rescaled to agree with the observed excess. For example, the excess seen at $m_H \sim 160 \text{ GeV}/c^2$, although giving formally a low “local” p -value, actually is not too consistent with the SM Higgs as the best-fit $\hat{\mu}$ is too small. Similarly, the $m_H \sim 120 \text{ GeV}/c^2$ excess does not seem to fit the standard model Higgs either as it requires an about two times larger cross section.

Overall, in the high mass region, above $200 \text{ GeV}/c^2$, the data agree well with the expectations for the background-only hypothesis. The few excesses observed in the low mass region are rather modest. Background fluctuations are assessed to have fair chances to be responsible for them. Hence, the only solid conclusion we can derive from the present search results are exclusion limits as reported above. More data, now rapidly coming, will increase the statistical accuracy of the existing analyses and allow us to introduce further improvements in search strategies. Both will help understand the nature of the observed excesses (if they remain after adding more data) and substantially improve the sensitivity of our SM Higgs searches.

4.3 Combination results: search for the SM4 Higgs boson

Finally, we perform the combination of the six analyses in the context of the standard model with four generations of fermions (SM4). In such a scenario, the $gg \rightarrow H$ cross section receives a large boost due to the presence of the 2 additional heavy quarks. The benchmark masses for the 4th generation fermions, and corresponding changes in Higgs production cross sections and branching ratios, are provided by the LHC Higgs Cross Section Group [29]. Figure 22 shows the observed 95% C.L. upper limits on the signal strength modifier $\mu^{95\%CL}$ as a function of the SM4 Higgs boson mass, where μ is now defined with respect to the SM4 Higgs cross section, namely: $\mu = \sigma/\sigma_{SM4}$. One can see that the Higgs boson hypothesis in the 4-generation standard model is excluded in the mass range from $120 \text{ GeV}/c^2$ to $600 \text{ GeV}/c^2$ (maximum Higgs boson mass covered by the current analyses). Making the 4th generation fermions heavier results in somewhat smaller cross sections at high masses [30], but not sufficiently low to affect the exclusion range.

between each other and from the combined fit $\hat{\mu}$. Second, there are many correlated systematic errors between channels that can be accounted for only in the proper combination with access to the full information.

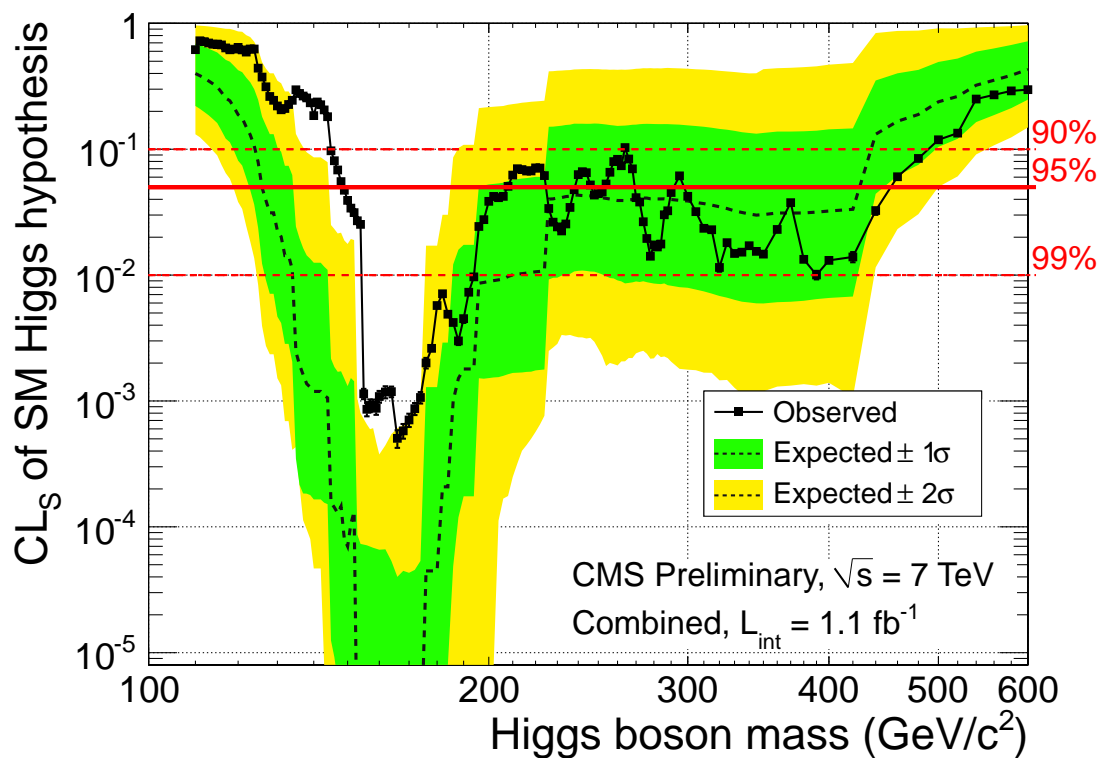


Figure 17: The CL_s value for the standard model Higgs hypothesis as a function of the Higgs boson mass in the range 110-600 GeV/c^2 . The observed values are shown by a solid line. The dashed black line indicates the median expected CL_s value for the background-only hypothesis, while the green/yellow bands indicate the ranges that are expected to contain 68%/95% of all observed limit excursions from the median. The three red horizontal lines show confidence levels of 90%, 95%, and 99% defined as $(1 - CL_s)$.

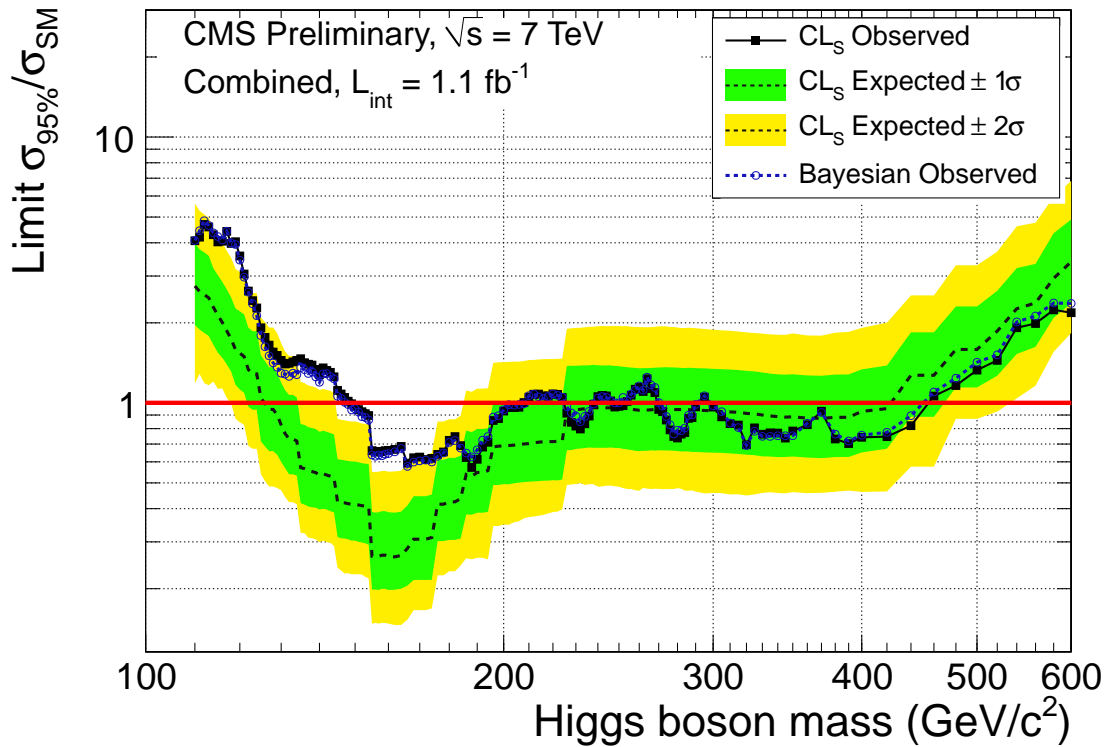


Figure 18: The combined 95% C.L. upper limits on the signal strength modifier $\mu^{95\%CL}$, where $\mu = \sigma/\sigma_{\text{SM}}$, as a function of the SM Higgs boson mass in the range 110-600 GeV/c^2 . The observed limits are shown by solid symbols and black line. The observed limits inferred from the Bayesian approach are shown as open circles. The dashed line indicates the median expected $\mu^{95\%CL}$ value for the background-only hypothesis, while the green/yellow bands indicate the ranges that are expected to contain 68%/95% of all observed limit excursions from the median. Both bands and the median are shown for the CL_s method.

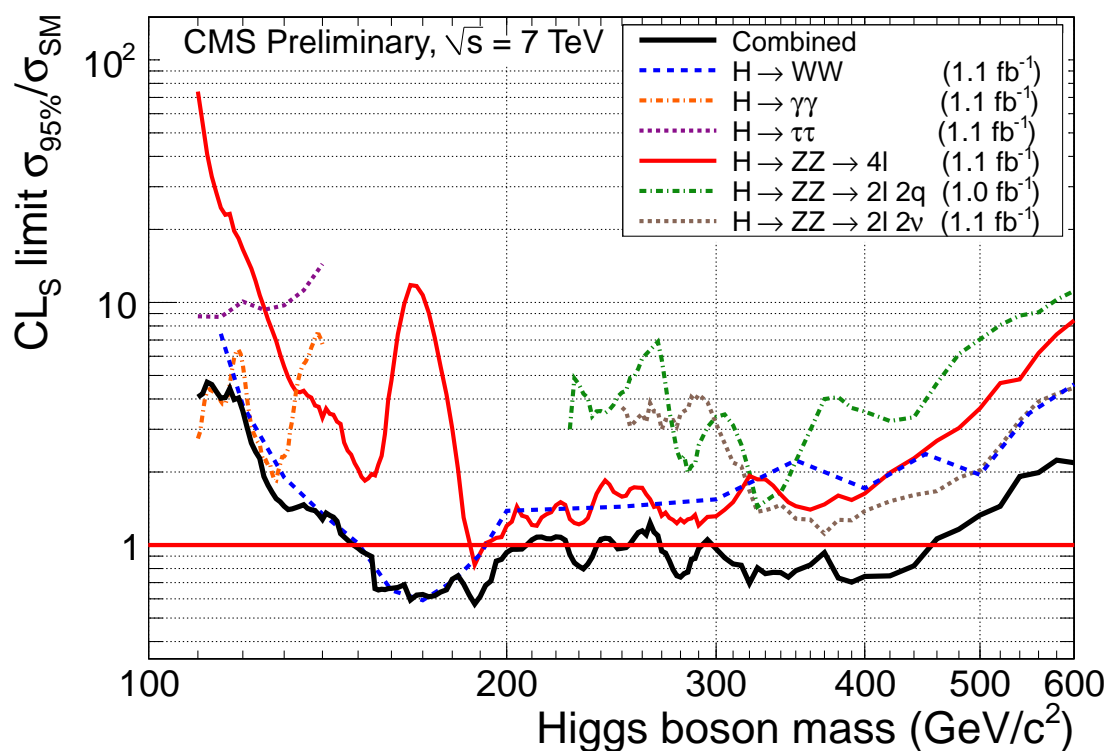


Figure 19: The observed 95% C.L. upper limits on the ratio of the excluded to standard model cross sections $\mu = \sigma_H^{95\%CL} / \sigma_H^{SM}$ as a function of the SM Higgs boson mass in the range 110-600 GeV/ c^2 for the six major analyses and their combination. The limits are obtained with the CL_s method as described in Sec. 2.

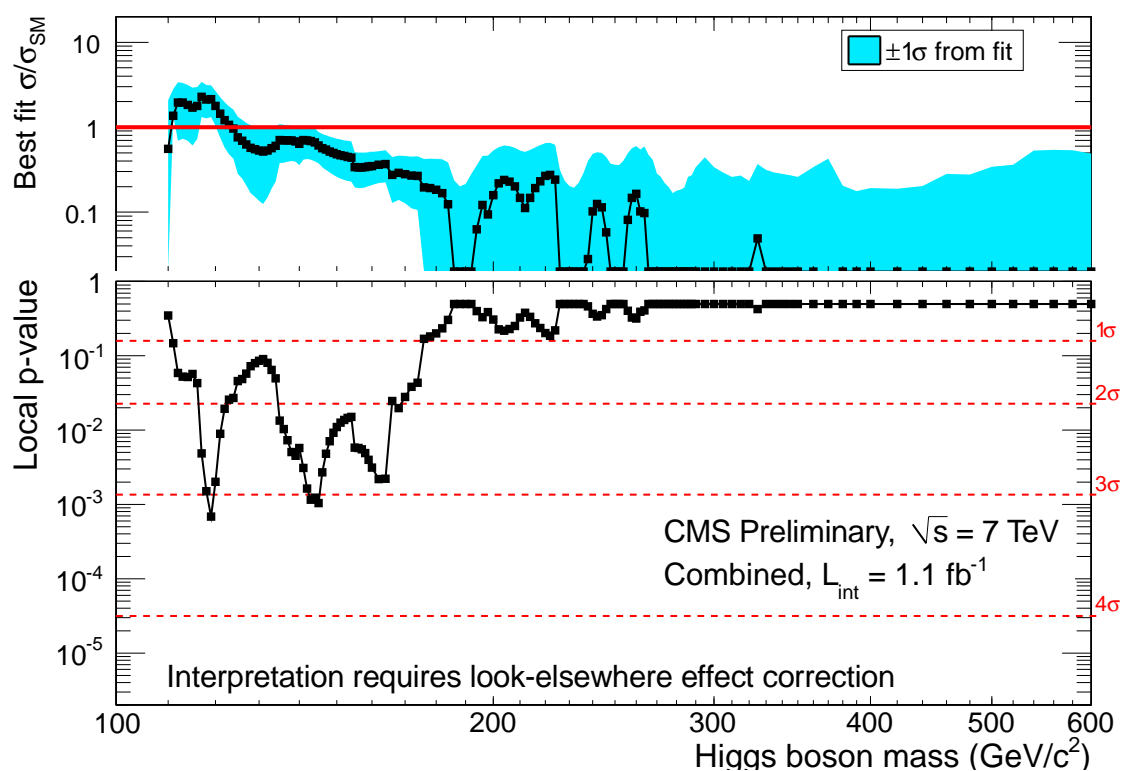


Figure 20: The observed best-fit signal strength $\hat{\mu} = \sigma/\sigma_{SM}$ (top) and an estimate of “local” \tilde{p} -values (bottom) vs Higgs boson mass. The \tilde{p} -value is an estimated probability of upward background fluctuations as high or higher than the excesses observed in data. It has to be further de-rated by the trial factor of a yet undetermined scale (analyses used in the combination have been shown to have the trial factors ranging from $O(1)$ - $O(100)$). The $\hat{\mu}$ value indicates by what factor the SM Higgs cross section would have to be rescaled to best match the observed data.

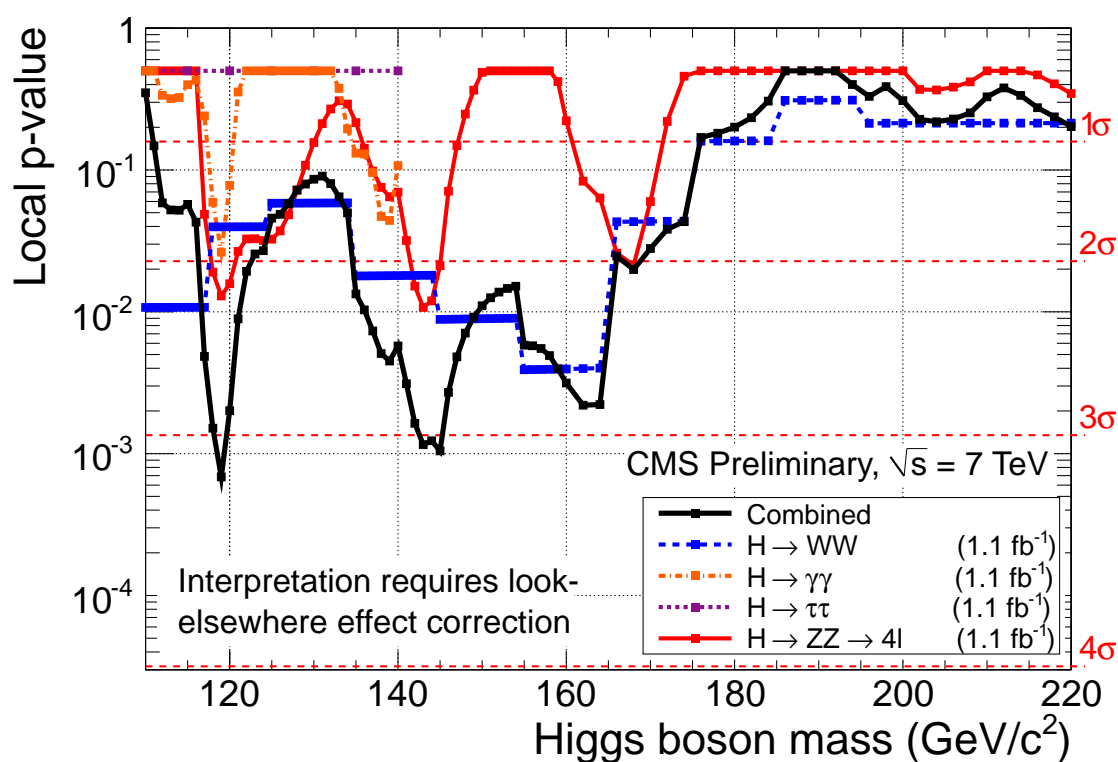


Figure 21: Estimated "local" \tilde{p} -values vs Higgs boson mass. The \tilde{p} -value is an estimated probability of upward background fluctuations as high or higher than the excesses observed in data. It has to be further de-rated by the trial factor of yet not determined scale (analyses used in the combination have been shown to have the trial factors ranging from O(1)-O(100)).

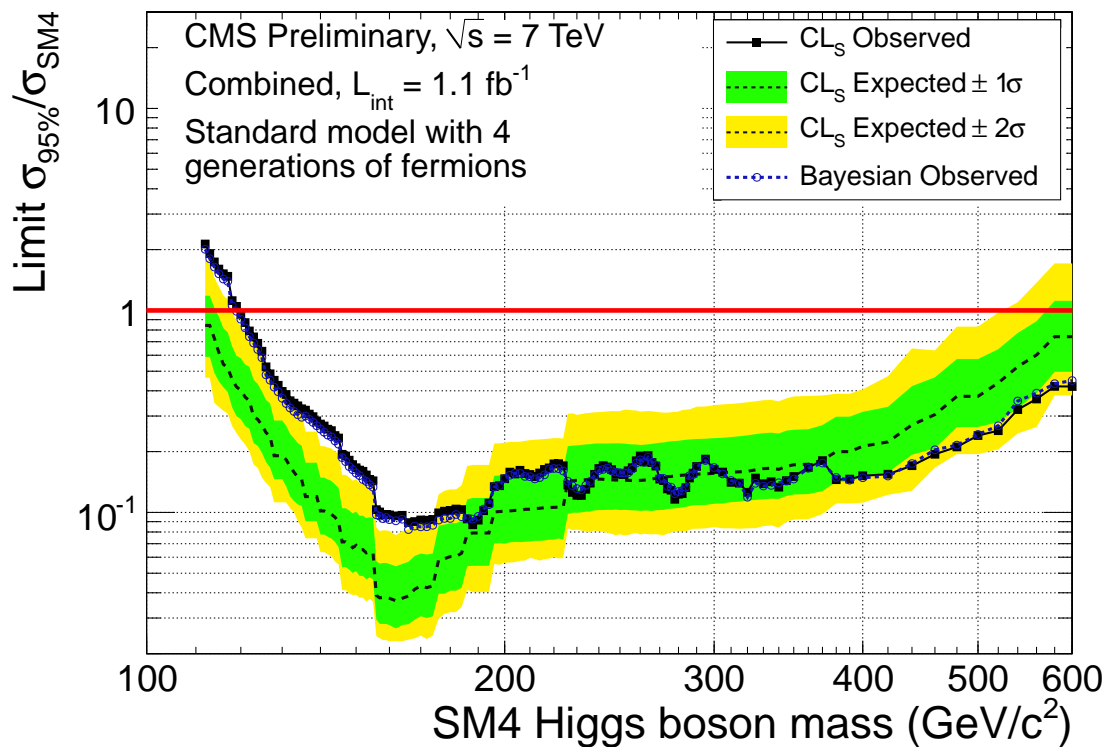


Figure 22: The combined 95% C.L. upper limits on the signal strength modifier $\mu^{95\%CL}$, where $\mu = \sigma/\sigma_{\text{SM4}}$, as a function of the SM4 Higgs boson mass in the range 110-600 GeV/c^2 . The observed CL_s -based limits are shown by the solid symbols and black line and exclude the SM4 Higgs with a mass from 120 GeV/c^2 to 600 GeV/c^2 (maximum Higgs boson mass covered by the current analyses). The Bayesian limits are shown with open symbols and give nearly identical results.

5 Conclusions

The CMS Collaboration has searched for the SM Higgs boson in pp collisions at a center-of-mass energy of 7 TeV in six distinct Higgs decay final states: $H \rightarrow \gamma\gamma$, $H \rightarrow \tau\tau$, $H \rightarrow WW \rightarrow 2\ell 2\nu$, $H \rightarrow ZZ \rightarrow 4\ell$, $H \rightarrow ZZ \rightarrow 2\ell 2\nu$, and $H \rightarrow ZZ \rightarrow 2\ell 2q$. The amount of data used in these searches corresponds to $1.0\text{--}1.1 \text{ fb}^{-1}$. The Higgs boson mass range covered by these analyses spans from 110 to 600 GeV/c^2 . To increase the overall experimental sensitivity to the presence of the signal, the search results obtained in these six analyses have been further combined. The conclusion of this combination is that the SM Higgs boson is excluded at 95% C.L. in two mass ranges 149-206 and 300-440 GeV/c^2 , as well as several narrower intervals in between. The expected exclusion in the absence of a signal is 127-420 GeV/c^2 . At 90% C.L., we exclude the SM Higgs boson in the mass range from 145-480 GeV/c^2 .

The same experimental search results, reinterpreted in the context of the standard model with 4 fermion generations (SM4), allow us to exclude the SM4 Higgs boson with a mass in the range 120-600 GeV/c^2 at 95% C.L.

Acknowledgments

We would like to acknowledge the very fruitful and collaborative effort of the LHC Higgs Combination Group, to which some of us formally belong.

References

- [1] R. Barate and others (LEP Working Group for Higgs boson searches and ALEPH, DELPHI, L3, and OPAL Collaborations), "Search for the standard model Higgs boson at LEP", *Phys. Lett.* **B565** (2003) 61–75, [arXiv:hep-ex/0306033](https://arxiv.org/abs/hep-ex/0306033).
doi:10.1016/S0370-2693(03)00614-2.
- [2] CDF and D0 Collaborations, "Combined CDF and D0 Upper Limits on Standard Model Higgs Boson Production with up to 8.2 fb⁻¹ of Data", [arXiv:1103.3233](https://arxiv.org/abs/1103.3233).
- [3] The ALEPH, CDF, D0, DELPHI, L3, OPAL, SLD Collaborations, the LEP Electroweak Working Group, the Tevatron Electroweak Working Group, and the SLD electroweak and heavy flavour groups, "Precision Electroweak Measurements and Constraints on the Standard Model", *CERN-PH-EP-2010-095*,
<http://lepewwg.web.cern.ch/LEPEWWG/plots/summer2010/>, <http://arxiv.org/abs/1012.2367> (2010).
- [4] CMS Collaboration, "The CMS experiment at the CERN LHC", *JINST* **3** (2008) S08004.
doi:10.1088/1748-0221/3/08/S08004.
- [5] CMS Collaboration, "Search for the standard model Higgs Boson in the decay channel $H \rightarrow \gamma\gamma$ at CMS", *CMS PAS HIG HIG-11-010* (2011).
- [6] CMS Collaboration, "Search for the Higgs Boson in the decay channel $H \rightarrow \tau\tau$ at CMS", *CMS PAS HIG HIG-11-009* (2011).
- [7] CMS Collaboration, "Search for the standard model Higgs Boson in the decay channel $H \rightarrow WW \rightarrow 2\ell 2\nu$ at CMS", *CMS PAS HIG HIG-11-003* (2011).
- [8] CMS Collaboration, "Search for the standard model Higgs Boson in the decay channel $H \rightarrow ZZ \rightarrow 4\ell$ at CMS", *CMS PAS HIG HIG-11-004* (2011).

-
- [9] CMS Collaboration, “Search for the standard model Higgs Boson in the decay channel $H \rightarrow ZZ \rightarrow 2\ell 2\nu$ at CMS”, *CMS PAS HIG HIG-11-005* (2011).
- [10] CMS Collaboration, “Search for the standard model Higgs Boson in the decay channel $H \rightarrow ZZ \rightarrow \ell^- \ell^+ q\bar{q}$ at CMS”, *CMS PAS HIG HIG-11-006* (2011).
- [11] LHC Higgs Cross Section Working Group, S. Dittmaier, C. Mariotti et al., “Handbook of LHC Higgs Cross Sections: 1. Inclusive Observables”, *CERN-2011-002* (CERN, Geneva, 2011) [arXiv:1101.0593](https://arxiv.org/abs/1101.0593).
- [12] ATLAS Collaboration, CMS Collaboration, and LHC Higgs Combination Group, “Procedure for the LHC Higgs boson search combination in summer 2011”, (July, 2011).
- [13] T. Junk, “Confidence level computation for combining searches with small statistics”, *Nucl.Instrum.Meth.* **A434** (1999) 435–443, [arXiv:hep-ex/9902006](https://arxiv.org/abs/hep-ex/9902006).
[doi:10.1016/S0168-9002\(99\)00498-2](https://doi.org/10.1016/S0168-9002(99)00498-2).
- [14] A. L. Read, “Modified frequentist analysis of search results (the CLs method)”, *CERN Yellow Report CERN-2000-005* (2000) 81.
- [15] A. L. Read, “Presentation of search results: the CLs technique”, *J. Phys. G: Nucl. Part. Phys.* **28** (2002) 2693.
- [16] W. Fisher, “Systematics and Limit Calculations”, (2006). Report No. FERMILAB-TM-2386-E.
- [17] W. Fisher, “Collie: A Confidence Level Limit Evaluator”, (June, 2009). D0 note 5595.
- [18] T. Junk, “Sensitivity, Exclusion and Discovery with Small Signals, Large Backgrounds, and Large Systematic Uncertainties”, (October, 2007).
CDF/DOC/STATISTICS/PUBLIC/8128.
- [19] A. O’Hagan and J.J. Forster, “Kendall’s Advanced Theory of Statistics. Vol. 2B: Bayesian Inference”. Arnold, London, 2004.
- [20] S. Wilks, “The large-sample distribution of the likelihood ratio for testing composite hypotheses”, *Ann. Math. Statist.* **9** (1938) 60.
- [21] L. Moneta, K. Belasco, K. Cranmer et al., “The RooStats Project”, in *13th International Workshop on Advanced Computing and Analysis Techniques in Physics Research (ACAT2010)*. SISSA, 2010. [arXiv:1009.1003](https://arxiv.org/abs/1009.1003). PoS(ACAT2010)057.
- [22] Chen, M. and Korytov, A., “Limits and Significance”.
<https://mschen.web.cern.ch/mschen/LandS/>.
- [23] S. Alioli, P. Nason, C. Oleari and E. Re, “A general framework for implementing NLO calculations in shower Monte Carlo programs: the POWHEG BOX”, *JHEP*.
- [24] T. Sjöstrand et al., “PYTHIA”, *Comput. Phys. Commun.* **135** (2001) 238.
- [25] D. d. F. G. Bozzi, S. Catani and M. Grazzini *Phys. Lett.* **B** (2003), no. 564, 65.
- [26] S. Bernstein, “Démonstration du théorème de Weierstrass fondée sur le calcul des probabilités”, *Comm. Soc. Math. Kharkov* **13** (1912) 1.

-
- [27] J. Campbell and R. K. Ellis *Nucl. Phys. Proc. Suppl.* **205-206** (2010) 10–15. MCFM code: <http://mcfm.fnal.gov/>.
- [28] CMS Collaboration, “CMS technical design report, volume II: Physics performance, Appx 2”, *J. Phys. G* **34** (2007) 995–1579.
- [29] LHC Higgs Cross Section Working Group, “Fourth Generation Model”, <https://twiki.cern.ch/twiki/bin/view/LHCPhysics/SM4At7TeV>.
- [30] N. Becerici Schmidt, S.A. Çetin, S. Istin, S. Sultansoy, “The fourth Standard Model family and the competition in Standard Model Higgs boson search at Tevatron and LHC”, *Eur.Phys.J. C* (2010), no. 66, 119.